



Biological aggregations from spatial memory and nonlocal advection

Di Liu ^{a,b,1}, Jonathan R. Potts ^c, Yuriy Salmaniw ^{d,b,*}, Junping Shi ^e, Hao Wang ^f

^a School of Mathematics, Hangzhou Normal University, Hangzhou, 311121, PR China

^b School of Mathematics and Statistics, Central South University, Changsha, 410083, PR China

^c School of Mathematical and Physical Sciences, University of Sheffield, Sheffield, United Kingdom

^d Mathematical Institute, University of Oxford, Oxford, United Kingdom

^e Department of Mathematics, William & Mary, Williamsburg, VA 23187-8795, USA

^f Department of Mathematical and Statistical Sciences, University of Alberta, Edmonton, AB T6G 2G1, Canada

ARTICLE INFO

Communicated by Matthew Simpson

Keywords:

Nonlocal advection

Bifurcation analysis

Spatial memory

Pattern formation

ABSTRACT

We investigate a nonlocal reaction–diffusion–advection model of a population of organisms that integrates spatial memory of previously visited locations and nonlocal detection in space, resulting in a coupled PDE–ODE system reflective of several models found in spatial ecology. Our study advances the mathematical understanding of such models by proving the existence and uniqueness of a global weak solution in one spatial dimension using an iterative approach. This result includes potentially discontinuous detection kernels, explicitly emphasizing the so-called ‘top-hat’ detection function, and does not place any restriction on the rate of advection, thereby addressing some analytical voids in the mathematical discourse on such models. A comprehensive spectral and stability analysis is also performed, providing analytical expressions for bifurcation values contingent on various model parameters, such as species advection rate, diffusion rate, memory uptake and decay rates. Unlike classical reaction–diffusion systems, the point spectrum may now include elements that have an infinite-dimensional kernel. We show the existence of such a point and that it remains negative, ensuring that it does not influence the stability of the constant steady state. Linear stability analysis then provides critical values for destabilizing the constant steady state. We explicitly describe the form of the non-constant steady state near these critical values and classify the nature of the pitchfork bifurcation as forward/backward and stable/unstable. To complement our analytical insights, we explore a targeted case study of three particular instances with the top-hat detection function. Using a pseudo-spectral method, we depict a numerical bifurcation diagram showing cases with sub or supercritical behaviour.

1. Introduction

1.1. Background and model formulation

Spatial memory is a key feature driving the movement of mobile organisms [1]. As organisms move, they gather information about where they have been, building a map that informs future movement decisions. This process generates a feedback mechanism whereby previous visitations of favourable locations can cause repeated visits, resulting in the organism confining itself to certain specific areas of the landscape. In animal ecology, such memory processes are considered foundational in the construction of home ranges [2–4], small areas where an animal decides to perform its daily activities instead of roaming more widely. Conversely, memory of unfavourable locations can cause animals to relocate. For example, memory has been shown to

play a key role in migratory movements [5,6] and avoiding conspecifics to form territories or home ranges [7,8].

Understanding how memory processes help to shape the space use of animals is thus becoming a question of increasing interest in both empirical ecology [1,9–11] and mathematical modelling [7,12–15]. From a modelling perspective, a key tool for modelling movement in response to remembered space use is via an advection term in a partial differential equation (PDE). This advection term is typically nonlocal in space, for both biological and mathematical reasons. From a biological perspective, nonlocality is important because organisms will generally sense their surrounding environment – for example, through sight, smell, or touch – and make movement decisions accordingly [16,17]. Moreover, this nonlocality occurs not only in animals but also in cells [18,19]. Mathematically, nonlocal advection is often crucial for well-posedness and avoiding blow-up of PDEs [20,21].

* Corresponding author at: Mathematical Institute, University of Oxford, Oxford, United Kingdom.

E-mail address: salmaniw@maths.ox.ac.uk (Y. Salmaniw).

¹ Co-first author.

Alongside advection, mathematical models of organism movement typically have a diffusive term, accounting for the aspects of movement that we are not explicitly modelling (such as foraging), and may also have a reaction term representing the births and deaths of organisms. This leads to the formalism of reaction–diffusion–advection equations (RDAs). In a one-dimensional spatial domain Ω , such an RDA might have the following general form

$$u_t = du_{xx} + \alpha(ua_x)_x + f(u), \quad x \in \Omega, \quad t > 0. \quad (1.1)$$

Here, $d > 0$ denotes the rate of diffusion (exploratory movement), $\alpha \in \mathbb{R}$ denotes the rate of advection towards ($\alpha < 0$) or away from ($\alpha > 0$) the environmental covariates described by the function $a(x, t)$, and $f(u)$ describes population changes through birth/death processes. When paired with an appropriate initial/boundary condition, we seek to analyse dynamical behaviours of the solution $u(x, t)$ as it depends on parameters appearing in the equation.

The aspect of memory then appears in the advection term $a(x, t)$. A recent review paper by Wang and Salmaniw [13] covers in detail the development of equations to model memory, as well as the related concept of learning, along with a large collection of open problems and directions in this area. The central idea is to model spatial memory as a map, $k(x, t)$, which evolves over time as the organism learns about its environment [1,7,22]. This map may represent something in the mind of a specific animal, sometimes called a ‘cognitive map’ [23,24], or it could represent the memory of past animal locations embedded in the environment, e.g. due to animals depositing scent marks or forging trails.

Here, we seek to explore the influence of such a map on the space-use patterns of a single population, u . To this end, we describe the evolution of $k(x, t)$ through the ordinary differential equation for each $x \in \Omega$, following [7]

$$k_t = g(u) - (\mu + \beta u)k, \quad t > 0. \quad (1.2)$$

Here, the function $g(\cdot)$ describes the uptake rate of the map k as it depends on the population $u(x, t)$; $\mu \geq 0$ describes the rate at which memories fade over time; and $\beta \geq 0$ describes a rate at which organisms remove a location from their memory map on revisitation (e.g. if animals want to avoid overuse of a location [25]).

Note that, for simplicity, we have assumed that all organisms in a population share a common memory map. This makes it perhaps more amenable to modelling the distribution of cues left on the environment, e.g. scent marks or visual cues [26,27], rather than memory contained in the minds of animals. Alternatively, if the population modelled by $u(x, t)$ has some process of relatively rapid information sharing, then we can view $k(x, t)$ as a shared memory amongst the population (e.g. for social insects, this may be valid). As another example, if $u(x, t)$ is the probability distribution of a single animal (in which case $f(u) = 0$ per force), then $k(x, t)$ can be used to model a map in the mind of an individual [7].

Prototypical examples of the function $g(u)$ might be $g(u) = \rho u$, denoting memory accruing in proportion to animal visitations, or $g(u) = \rho u^2$, denoting uptake of memory when members of u encounter one another (here, ρ is a constant). However, these can, in principle, lead to unbounded memory. Therefore, we can either take another functional form, such as $g(u) = \rho u^2 / (1 + cu)$ (cf. the Holling type II functional response [28]), or modify Eq. (1.2) to the following as in [7]:

$$k_t = g(u)(\kappa - k) - (\mu + \beta u)k, \quad t > 0, \quad (1.3)$$

where $\kappa > 0$ denotes a theoretical maximal memory capacity.

To combine this mechanism of spatial memory with nonlocal perception, we model nonlocal effects through a spatial convolution:

$$\bar{k}(x, t) = (G * k)(x, t) = \frac{1}{|\Omega|} \int_{\Omega} G(x - y)k(y, t)dy. \quad (1.4)$$

Here, the function $G(\cdot)$ is referred to as a *perceptual kernel* or *detection function*, which describes how an animals’ ability to perceive landscape information varies with distance [13,29]. Common forms of the

detection function $G(\cdot)$ include the *Gaussian* detection function, the *exponential* detection function, or the *top-hat* detection function, each taking the respective forms in $\Omega = \mathbb{R}$:

$$G(x) := \frac{1}{\sqrt{2\pi}R} e^{-x^2/2R^2}, \quad (1.5)$$

$$G(x) := \frac{1}{2R} e^{-|x|/R}, \quad (1.6)$$

$$G(x) := \begin{cases} \frac{1}{2R}, & -R \leq x \leq R, \\ 0, & \text{otherwise.} \end{cases} \quad (1.7)$$

Here, $R \geq 0$ is referred to as the *perceptual radius* [13] (also referred to as the *detection scale* [29]) which is meant to model the *perceptual range* of the organism: *the distance from which a particular landscape element can be perceived as such (or detected) by a given animal* [30]. In the context of detecting animals in an environment, the function $G(x)$ is meant to describe the probability of detecting an organism given a distance from the point of observation [31, Fig. 3.15]. The parameter R then modulates this probability of detection. The Gaussian detection function provides the most information far away from the location of observation, whereas the top-hat detection function places an absolute limit on how far the organism can detect information. Even within the same organism, it is known that different detection mechanisms may yield different perceptual ranges. For example, bats use echolocation for short-range detection (of, e.g., insects) while they use vision to detect larger landscape elements (e.g., forest edges) [32].

In general, it is reasonable to assume the detection function satisfies

- (i.) $G(x)$ is even (symmetric about the origin);
- (ii.) $\int_{\mathbb{R}} G(x)dx = 1$;
- (iii.) $\lim_{R \rightarrow 0^+} G(x) = \delta(x)$;
- (iv.) $G(x)$ is non-increasing from the origin.

Here, $\delta(x)$ denotes the Dirac-delta distribution. Each of the Gaussian, exponential, and top-hat kernels satisfy these properties over \mathbb{R} ; appropriate modification is sometimes required in a bounded domain. Readers are encouraged to review [13,29] for further discussion on detection kernels and some of the challenges in defining nonlocal kernels near a boundary region.

Taking the advective potential $a(x, t) = \bar{k}(x, t)$, where k solves either (1.2) or (1.3), we combine the equation describing movement (1.1) with a dynamic spatial map in $\Omega = (-L, L)$, $L > 0$, to arrive at the following two systems of equations subject to periodic boundary conditions:

$$\begin{cases} u_t = du_{xx} + \alpha(u\bar{k}_x)_x + f(u), & x \in (-L, L), \quad t > 0, \\ k_t = g(u) - (\mu + \beta u)k, & x \in (-L, L), \quad t > 0, \end{cases} \quad (1.8.a)$$

and

$$\begin{cases} u_t = du_{xx} + \alpha(u\bar{k}_x)_x + f(u), & x \in (-L, L), \quad t > 0, \\ k_t = g(u)(\kappa - k) - (\mu + \beta u)k, & x \in (-L, L), \quad t > 0. \end{cases} \quad (1.8.b)$$

In either case, we denote by $u(x, 0) = u_0(x)$, $k(x, 0) = k_0(x)$ the initial data, chosen to be $2L$ -periodic in Ω . Both models can be viewed as a single-species analogue of the various multi-species models studied in, for example [22,33,34], for their broad applications to ecology and cell biology [19]. Due to the challenging nature of these multi-species PDE–ODE models, the novelty of the present work is in the rigorous treatment of the well-posedness of the problem for a single species and the detailed description of the rich bifurcation structure found in such problems.

As discussed in [13], boundary conditions in a nonlocal setting in a bounded domain are highly non-trivial in general. It is not clear how to appropriately define the spatial convolution (1.4) near the boundary of the domain (in a biological sense) while remaining analytically tractable. For this reason, we appeal to a periodic boundary condition, which requires no further modification of (1.4) near the

boundary points $\{-L, L\}$. While problems (1.8.a) and (1.8.b) appear similar in form, it is of interest to understand exactly when and how these two formulations differ in their solution behaviours: should they be identical, it seems reasonable to choose the more tractable model depending on the goals; should they differ significantly, it is reasonable to determine *when* and *how* they differ, which gives insights into the validity of either case in a given context.

There exist a number of works that consider a multi-species model of the form taken in either (1.8.a) or (1.8.b), see, e.g., [7,22]. In these works, a linear stability analysis is performed to determine conditions sufficient for pattern formation to occur. These models are comparable in that they include a cognitive map through an additional, dynamic equation, and they also incorporate nonlocal perception. Other models with nonlocal advective operators have been studied by [35–37], where some global existence results are obtained. In [35], fractional Sobolev spaces are utilized in a one-dimensional torus to establish a global existence result which includes the possibility of a top-hat kernel; however, the model does not incorporate a dynamic cognitive map. In [36], a global existence result is established using a contraction mapping argument, but the regularity requirements of the nonlocal kernel do not include the top-hat detection function. In [37], a global existence result is obtained for a special case of the n -species cross-diffusion system considered in [36], but the kernels are assumed to be *positive-definite* and in *detailed balance*. A positive-definite condition means that the Fourier coefficients are all non-negative, which rules out the top-hat detection function; a detailed balance condition rules out run-and-chase scenarios, for example, somewhat limiting biological application. Other memory-based movement models have been investigated in [38,39], where the cognitive map is now given by a nonlocal integral operator in *time*. In such cases, the problem is a delay partial differential equation. The stability of coupled PDE–ODE models has also been studied in works such as [40,41].

With our models at hand, the major goals of this paper are as follows. First, we seek to prove the well-posedness of models (1.8.a) and (1.8.b). In particular, in Section 2 we prove the existence of a unique, global weak solution when the detection function $G(\cdot)$ satisfies an L^p -embedding type condition (see Hypotheses (H3)), which includes the discontinuous top-hat detection function. This provides an answer to Open Problems 10 and 12 found in [13], at least for the single species case. We then shift our attention to the solution behaviour and the potential for pattern formation at a steady state. In Section 3–4, we perform a robust stability and bifurcation analysis to understand the long-term behaviour of the solution as it depends on parameters d , α , the uptake rate $g(\cdot)$ and the kernel $G(\cdot)$. While an intuitive understanding of the relevant factors influencing pattern formation can be gleaned from a less scrupulous linear stability analysis (see Section 3.2), further care is needed for nonlocal advective operators. There may exist elements belonging to the point spectrum with an infinite-dimensional kernel, and such elements are not detectable by classical linear stability analysis. If such an element has a nonnegative real part, then perturbations may grow, leading to instability even if all eigenvalues from the linear stability analysis suggest (local) stability. This is different from standard reaction–diffusion systems, for example, where all elements of the point spectrum correspond to a finite-dimensional kernel. In our case, we find that these values are indeed entirely negative and so have no impact on the stability of the homogeneous state. Section 5 is then dedicated to a detailed case study with the top-hat detection function. To explore the subtle differences in our formulations, we focus on three particular forms of uptake $g(\cdot)$ to better understand differences in fundamental assumptions for the function $g(\cdot)$. Numerical simulations using a pseudo-spectral method [13,36] with third-order strong-stability preserving Runge–Kutta (SSPRK3) time-stepping algorithm are presented in Section 5 to highlight these differences through numerical bifurcation diagrams depicting subcritical bifurcations for sublinear uptake rates $g(\cdot)$ (see Figs. 2–3) and supercritical bifurcations for linear uptake rates $g(\cdot)$ (see Figs. 5–6).

1.2. Preliminaries & hypotheses

Denote $\mathbb{N}_0 = \mathbb{N} \cup \{0\}$. Recall that the following eigenvalue problem

$$\begin{cases} -\phi''(x) = l\phi(x), & x \in (-L, L), \\ \phi(-L) = \phi(L), \quad \phi'(-L) = \phi'(L), \end{cases} \quad (1.8)$$

with eigenvalues and eigenfunctions

$$l_{\pm n} = \frac{n^2 \pi^2}{L^2}, \quad \phi_{\pm n}(x) = e^{\pm \frac{i n \pi}{L} x} = \cos\left(\frac{n \pi}{L} x\right) \pm i \sin\left(\frac{n \pi}{L} x\right), \quad n \in \mathbb{N}_0. \quad (1.9)$$

We define the linear spaces

$$L^2_{per}(-L, L) = \left\{ h \in L^2(-L, L) : h = \sum_{n=-\infty}^{\infty} c_n \phi_n \text{ with } \sum_{n=-\infty}^{\infty} |c_n|^2 < \infty \right\},$$

and

$$H^2_{per}(-L, L) = \{ h \in L^2_{per}(-L, L) : h'' \in L^2_{per}(-L, L) \},$$

where

$$c_n = \langle h, \phi_n \rangle = \frac{1}{2L} \int_{-L}^L h(x) \phi_{-n}(x) dx.$$

Note that L^2_{per} contains the periodic functions. We then denote by X and Y the spaces $H^2_{per}(-L, L) \times L^2_{per}(-L, L)$ and $L^2_{per}(-L, L) \times L^2_{per}(-L, L)$, respectively. We always assume the following for the spatial kernel G :

$$(H0) \begin{cases} G(x) \in L^1_{per}(-L, L), \quad G(-x) = G(x) \text{ for all } x \in (-L, L), \\ \int_{-L}^L G(y) dy = 1, \\ 0 < R < L, \end{cases}$$

where $2L$ is the length of the domain. The restriction on R ensures that the convolution of G with a nonconstant function over $(-L, L)$ is itself nonconstant.

The Gaussian and exponential detection functions each satisfy (H0) in $(-L, L)$ when the following additional prefactors are included: $R^{-2} \operatorname{erf}\left(\frac{L-R}{\sqrt{2}}\right)$ and $1 - e^{-L/R}$; however, it should be noted that these functional forms are most appropriately applied on the whole space. The top-hat detection function satisfies (H0) without further modification. For the stability and bifurcation analysis performed in Section 3–4, we assume that the growth rates f and g satisfy

- (H1) $f(u) \in C^3([0, \infty))$, $f(0) = f(1) = 0$, $f'(0) > 0$, $f'(1) < 0$, $f(u) > 0$ for $u \in (0, 1)$ and $f(u) < 0$ for $u > 1$.
- (H2) $g(u) \in C^3([0, \infty))$, $g(u) > 0$ on $(0, \infty)$, $g(0) = 0$, and $g(1) = \rho > 0$. In addition, we assume the non-degeneracy condition $g'(1) \neq \beta\rho/(\mu + \beta)$.

The non-degeneracy condition in (H2) ensures that key quantities remain well-defined; see, for example, Eq. (1.13). In fact, the sign of $g'(1) - \beta\rho/(\mu + \beta)$ determines whether the bifurcating solution u is in or out of phase with the spatial map k , see Theorems 1.5–1.6.

To establish the well-posedness of the problem, we also assume in addition to (H0) that the kernel $G(\cdot)$ satisfies the following L^p -type estimate for any $R > 0$ fixed:

$$(H3) \quad \|\bar{z}_x\|_{L^p(\Omega)} \leq C \|z\|_{L^p(\Omega)} \quad \text{for all } z \in L^p(\Omega), \quad 1 \leq p \leq \infty.$$

Hypothesis (H3) is appropriately generalizable as in [42, Hypothesis (H2)] for problems in higher dimensions.

A prototypical example of $f(u)$ is the logistic function $f(u) = u(1-u)$, foundational in models of population growth. Biologically-motivated examples of $g(u)$ include $g(u) = \rho u$, $g(u) = \rho u^2$, and $g(u) = \rho u^2/(1 + cu)$, which were discussed in the paragraph prior to Eq. (1.3). Note that the hypotheses required in the bifurcation analysis are generally stronger than those required for well-posedness; for this reason, we state the sufficient hypotheses for the existence of a solution directly in the statement of Theorem 1.1.

Throughout this paper, we denote the null space of a linear operator L by $\mathcal{N}(L)$, the domain of L by $\mathcal{D}(L)$, the range of L by $\mathcal{R}(L)$, the resolvent set of L by $\rho(L)$, and the spectrum of L by $\sigma(L)$. We always denote by $Q_T := \Omega \times (0, T) = (-L, L) \times (0, T)$.

1.3. Statement of main results

Our first result establishes the existence of a unique, nontrivial solution (u, k) . Due to the weak regularity assumption (H0) on the kernel $G(\cdot)$, we do not expect solutions to be classical necessarily. Denote by $h(u, k)$ the right-hand side of the equation for the map k in either (1.8.a) or (1.8.b). We call (u, k) a *weak solution* to either (1.8.a) or (1.8.b) if, given any test function $\phi_i \in L^2(0, T; H^1(\Omega))$, $i = 1, 2$, there holds

$$\iint_{Q_T} u_t \phi_1 dxdt + \iint_{Q_T} (du_x + \alpha u \bar{k}_x)(\phi_1)_x dxdt = \iint_{Q_T} f(u) \phi_1 dxdt, \tag{1.10}$$

$$\iint_{Q_T} k_t \phi_2 dxdt = \iint_{Q_T} h(u, k) \phi_2 dxdt, \tag{1.11}$$

and the initial data is satisfied in the sense of $H^1(\Omega)$ (in fact, the initial data will be satisfied in the sense of $C(\bar{\Omega})$ by the Sobolev embedding). We call a weak solution a *global weak solution* if (1.10)–(1.11) holds for any $T > 0$.

We have the following well-posedness result for problems (1.8.a) and (1.8.b).

Theorem 1.1. Fix $T > 0$, $\alpha \in \mathbb{R} \setminus \{0\}$, $d, R > 0$, $\mu, \beta, \kappa \geq 0$, and assume that the kernel $G(\cdot)$ satisfies (H0) and (H3). Suppose that for some $\sigma \in (0, 1)$, $f, g \in C^{2+\sigma}(\mathbb{R}^+)$ with $f(0) = g(0) = 0$. Assume that f satisfies the bound

$$f(z) \leq f'(0)z \quad \text{for all } z \geq 0,$$

while g satisfies the bounds

$$g(z) \leq N(1 + z^q) \quad \text{for all } z \geq 0, \\ |g'(z)| \leq \tilde{N}(1 + z^{\tilde{q}}) \quad \text{for all } z \geq 0,$$

for some constants $N, \tilde{N} > 0$, $q \geq 1$ and $\tilde{q} \geq 0$. Finally, assume that the initial data u_0, k_0 satisfy

$$0 < u_0(x), k_0(x) \in W^{1,2}(\Omega) \text{ are periodic in } \Omega.$$

Then, there exists a unique, global weak solution (u, k) solving problem (1.8.a) in the sense of (1.10)–(1.11) satisfying $u \geq 0, k \geq 0$ so long as there exists $M > 0$ so that

$$g(z) \leq M(\mu + \beta z) \quad \text{for all } z \geq 0.$$

For problem (1.8.b), there exists a unique, global weak solution in the sense of (1.10)–(1.11) satisfying $u \geq 0, k \geq 0$ with no further restriction on $g(\cdot)$ other than (H2). Moreover, in either case there holds

$$u \in L^\infty(0, T; L^p(\Omega)) \cap C^{\sigma, \sigma/2}(\bar{Q}_T), \quad u_x, u_t \in L^2(0, T; L^2(\Omega)), \\ k \in L^\infty(0, T; L^p(\Omega)) \cap C^{\sigma, \sigma/2}(\bar{Q}_T), \quad k_x, k_t \in L^\infty(0, T; L^2(\Omega)),$$

for any $1 < p \leq \infty$, for some $\sigma \in (0, 1/2)$, and the initial data is satisfied in the sense of $C(\bar{\Omega})$.

Remark 1.2. In the theorem above, we generally require some global polynomial growth control over the memory uptake function $g(\cdot)$. From this result, we see that problem (1.8.a) is significantly more restrictive than problem (1.8.b) in terms of further growth conditions on $g(\cdot)$. Indeed, the first case requires that the memory uptake behaves roughly linearly, particularly for large arguments, while the second case requires no further growth condition. From our previous discussion of biologically-motivated forms of $g(\cdot)$, we see that the forms $g(u) = \rho u$ and $g(u) = \rho u^2 / (1 + cu)$ satisfy the necessary conditions for either system. On the other hand, quadratic growth $g(u) = \rho u^2$ as described in [7] satisfies the conditions for system (1.8.b) but not (1.8.a). This highlights an essential key difference between these two problems regarding their well-posedness.

For the detection function G satisfying (H0), the Fourier coefficient $C_n(G)$ is defined for any $n \in \mathbb{N}$ as follows:

$$C_n(G) = \frac{1}{2L} \int_{-L}^L e^{-\frac{in\pi}{L}y} G(y) dy = \frac{1}{2L} \int_{-L}^L \cos\left(\frac{n\pi}{L}y\right) G(y) dy, \tag{1.12}$$

For $n \in \mathbb{N}$, if $C_n(G) \neq 0$, define

$$\alpha_n = \frac{-(\mu + \beta)^2}{[g'(1)(\mu + \beta) - \beta\rho]C_n(G)} \left(d - \frac{f'(1)}{l_n} \right). \tag{1.13}$$

Notice that α_n is well-defined under hypothesis (H3). Note also that $C_n(G)$ could be positive or negative. Define

$$\Sigma^+ := \{n \in \mathbb{N} : \alpha_n > 0\}, \quad \Sigma^- := \{n \in \mathbb{N} : \alpha_n < 0\}, \\ \alpha_r := \begin{cases} +\infty & \text{whenever } \Sigma^+ = \emptyset, \\ \min_{n \in \Sigma^+} \alpha_n & \text{otherwise,} \end{cases} \tag{1.14} \\ \alpha_l := \begin{cases} -\infty & \text{whenever } \Sigma^- = \emptyset, \\ \max_{n \in \Sigma^-} \alpha_n & \text{otherwise.} \end{cases}$$

Note that α_r, α_l are well-defined as $\sum_{n=-\infty}^{\infty} |C_n(G)|^2 < \infty$. Given a fixed, even kernel G that is non-increasing from the origin, α_l corresponds to the (first) critical value at which the homogeneous state is destabilized by attractive forces. On the other hand, α_r for G is equivalent to α_l for $-G$, a non-decreasing kernel. α_r is thus the (first) critical value at which the homogeneous state becomes destabilized by repulsive forces. As observed in [43], if Σ^+ is empty (Σ^- is empty), then no value of α can destabilize the homogeneous state due to repulsive (attractive) forces. Note finally that these conventions are flipped if we instead assume that G is non-decreasing from the origin.

Then, we have the following theorem regarding the stability of the unique constant positive steady state $U_* = (1, \rho / (\mu + \beta))$ with respect to (1.8.a).

Theorem 1.3. Assume that assumptions (H0)–(H2) are satisfied, and let $\Sigma^+, \Sigma^-, \alpha_l, \alpha_r$ be defined as in (1.14). Then

- (i) The constant steady state solution U_* is locally asymptotically stable with respect to (1.8.a) if $\alpha_l < \alpha < \alpha_r$.
- (ii) The constant steady state solution U_* is unstable with respect to (1.8.a) if $\alpha < \alpha_l$ or $\alpha > \alpha_r$.

Similarly, we define

$$\hat{\alpha}_n = \frac{-(\rho + \mu + \beta)^2}{\kappa[g'(1)(\mu + \beta) - \beta\rho]C_n(G)} \left(d - \frac{f'(1)}{l_n} \right), \tag{1.15}$$

and

$$\hat{\Sigma}^+ := \{n \in \mathbb{N} : \hat{\alpha}_n > 0\}, \quad \hat{\Sigma}^- := \{n \in \mathbb{N} : \hat{\alpha}_n < 0\}, \\ \hat{\alpha}_r := \begin{cases} +\infty & \text{whenever } \hat{\Sigma}^+ = \emptyset \\ \min_{n \in \hat{\Sigma}^+} \hat{\alpha}_n & \text{otherwise} \end{cases} \tag{1.16} \\ \hat{\alpha}_l := \begin{cases} -\infty & \text{whenever } \hat{\Sigma}^- = \emptyset, \\ \max_{n \in \hat{\Sigma}^-} \hat{\alpha}_n & \text{otherwise.} \end{cases}$$

Then we have the stability results for the unique constant positive steady state $\hat{U}_* = (1, \rho\kappa / (\rho + \mu + \beta))$ with respect to (1.8.b).

Theorem 1.4. Assume that assumptions (H0)–(H2) are satisfied, and let $\hat{\Sigma}^+, \hat{\Sigma}^-, \hat{\alpha}_l, \hat{\alpha}_r$ be defined as in (1.16). Then

- (i) The constant steady state solution \hat{U}_* is locally asymptotically stable with respect to (1.8.b) if $\hat{\alpha}_l < \alpha < \hat{\alpha}_r$.
- (ii) The constant steady state solution \hat{U}_* is unstable with respect to (1.8.b) if $\alpha < \hat{\alpha}_l$ or $\alpha > \hat{\alpha}_r$.

The quantities $\alpha_n(\hat{\alpha}_n)$ defined in (1.13) ((1.15)) are the critical parameter values such that the stability of the spatially-constant steady state changes, and they are also bifurcation points for (1.8.a) ((1.8.b)) where spatially non-homogeneous steady-state solutions bifurcate from the constant ones as found in the following Theorems.

Theorem 1.5. Assume that assumptions (H0)-(H2) are satisfied, and $n \in \mathbb{N}$ such that $C_n(G) \neq 0$. Then near $(\alpha, U) = (\alpha_n, U_*)$, Eq. (1.8.a) has a line of homogeneous solutions $\Gamma_0 := \{(\alpha, U_*) : \alpha \in \mathbb{R}\}$ and a family of non-constant steady state solutions bifurcating from Γ_0 at $\alpha = \alpha_n$ in a form of

$$\Gamma_n := \{(\alpha_n(s), u_n(s, \cdot), k_n(s, \cdot)) : -\delta < s < \delta\} \tag{1.17}$$

with

$$\begin{cases} \alpha_n(s) = \alpha_n + \alpha'_n(0)s + o(s), \\ u_n(s, x) = 1 + s \cos\left(\frac{n\pi}{L}x\right) + s^2 z_{1n}(s, x), \\ k_n(s, x) = \frac{\rho}{\mu + \beta} + s \frac{g'(1)(\mu + \beta) - \beta\rho}{(\mu + \beta)^2} \cos\left(\frac{n\pi}{L}x\right) + s^2 z_{2n}(s, x), \end{cases} \tag{1.18}$$

where $z_n(s) = (z_{1n}(s, \cdot), z_{2n}(s, \cdot))$ satisfies $\lim_{s \rightarrow 0} \|z_n(s)\| = 0$. Moreover the set of steady state solutions of (1.8.a) near (α_n, U_*) consists precisely of the curves Γ_0 and Γ_n .

Theorem 1.6. Assume that assumptions (H0)-(H2) are satisfied, and $n \in \mathbb{N}$ such that $C_n(G) \neq 0$. Then near $(\hat{\alpha}, \hat{U}) = (\hat{\alpha}_n, \hat{U}_*)$, Eq. (1.8.b) has a line of homogeneous solutions $\hat{\Gamma}_0 := \{(\alpha, \hat{U}_*) : \alpha \in \mathbb{R}\}$ and a family of non-constant steady state solutions bifurcating from $\hat{\Gamma}_0$ at $\alpha = \hat{\alpha}_n$ in a form of

$$\hat{\Gamma}_n := \{(\hat{\alpha}_n(s), \hat{u}_n(s, \cdot), \hat{k}_n(s, \cdot)) : -\delta < s < \delta\} \tag{1.19}$$

with

$$\begin{cases} \hat{\alpha}_n(s) = \hat{\alpha}_n + \hat{\alpha}'_n(0)s + o(s), \\ \hat{u}_n(s, x) = 1 + s \cos\left(\frac{n\pi}{L}x\right) + s^2 \hat{z}_{1n}(s, x), \\ \hat{k}_n(s, x) = \frac{\rho}{\rho + \mu + \beta} + \kappa s \frac{g'(1)(\mu + \beta) - \beta\rho}{(\mu + \beta + \rho)^2} \cos\left(\frac{n\pi}{L}x\right) + s^2 \hat{z}_{2n}(s, x), \end{cases} \tag{1.20}$$

where $\hat{z}_n(s) = (\hat{z}_{1n}(s, \cdot), \hat{z}_{2n}(s, \cdot))$ satisfies $\lim_{s \rightarrow 0} \|\hat{z}_n(s)\| = 0$. Moreover the set of steady state solutions of (1.8.b) near $(\hat{\alpha}_n, \hat{U}_*)$ consists precisely of the curves $\hat{\Gamma}_0$ and $\hat{\Gamma}_n$.

We also classify the nature of the bifurcation at these critical values, see Theorems 4.4 and 4.5. Together, these results show that the central quantity governing spontaneous pattern formation is the advective strength towards or away from memorized areas, encapsulated in α . As $\alpha_l < 0 < \alpha_r$, holds necessarily from the assumptions made, the key driver of pattern formation is that α is of sufficient magnitude. If α is negative and G non-increasing from the origin, then we have an attraction towards remembered areas, similar to many nonlocal models of biological aggregation (e.g. [44]). Some examples are found in Figs. 2, 5, where patterns appear due to attractive forces. On the flip-side, positive α indicates repulsion from remembered areas and leads to patterns such as in Figs. 3, 6, where they emerge due to repulsive forces. Interestingly, there is a lack of symmetry in the sense that $-\alpha_l \neq \alpha_r$ in general. In fact, $|\alpha_l|$ and α_r do not even remain ordered! This can be seen in Figs. 1 and 4.

Moreover, Theorems 1.5 and 1.6 show the steady state consists of a single cosine wave near the bifurcation point, and Theorems 4.4 and 4.5 give conditions on the stability of the emergent branches. An example of subcritical bifurcations is shown in Figs. 2–3, whereas an example of supercritical bifurcations is shown in Figs. 5–6. For the first (unstable) case, we do not see the low-amplitude cosine wave emerge as a stable solution; instead, we observe an immediate jump to a high-amplitude solution. For the second (stable) case, we observe a stable, low-amplitude solution emerge smoothly from the homogeneous state.

2. Well-posedness

In this section, we prove the existence of a unique global solution to a problem more general than system (1.8.a) or (1.8.b) for detection functions $G(\cdot)$ satisfying (H0) and (H3), which includes the top-hat kernel. The restrictions on the growth terms $f(\cdot)$ and $g(\cdot)$ are compatible with the choices made in Section 5. The challenge is in treating the (potentially) discontinuous kernel appearing inside the nonlocal advection term. To overcome these difficulties, we abuse a useful ‘embedding’ property of the top-hat kernel in one spatial dimension. This allows one to obtain *a priori* estimates on the solution $k(x, t)$ from which we obtain appropriate uniform bounds on $u(x, t)$ and higher derivatives. We begin with some preliminary estimates.

2.1. Preliminary estimates

In general, we assume $G(\cdot)$ satisfies (H3); we first show this holds for the top-hat kernel.

Lemma 2.1. Let $1 \leq p \leq \infty$ and fix $T > 0$. Suppose $z(\cdot, t) \in L^p(\Omega)$ is periodic in Ω for almost every $t \in [0, T]$. Denote by $\bar{z}_x(\cdot, t)$ the spatial convolution (1.4) of z_x with the top-hat detection function. Then, for almost every $t \in [0, T]$ there holds

$$\|\bar{z}_x(\cdot, t)\|_{L^p(\Omega)} \leq \frac{1}{2RL} \|z(\cdot, t)\|_{L^p(\Omega)}. \tag{2.1}$$

In particular, we have that

$$\text{ess sup}_{t \in (0, T)} \|\bar{z}_x(\cdot, t)\|_{L^p(\Omega)} \leq (2RL)^{-1} \text{ess sup}_{t \in (0, T)} \|z(\cdot, t)\|_{L^p(\Omega)}, \tag{2.2}$$

for any $T > 0$ fixed.

Remark 2.2. If $z(\cdot, t)$ is continuous, we may replace ‘almost every’ with ‘every’ and ess sup with sup . This will be the case in the forthcoming results.

Proof. First, we drop the dependence on t for notational brevity. The result essentially follows from an elementary inequality and the fact that

$$\bar{z}_x = \frac{z(x+R) - z(x-R)}{4RL}$$

when $G(\cdot)$ is the top hat detection function. Consequently,

$$\begin{aligned} \|\bar{z}_x\|_{L^p(\Omega)}^p &= \frac{1}{(4RL)^p} \int_{\Omega} |z(x+R) - z(x-R)|^p dx \\ &\leq \frac{2^{p-1}}{(4RL)^p} \int_{\Omega} (|z(x+R)|^p + |z(x-R)|^p) dx \leq \frac{1}{(2RL)^p} \|z\|_{L^p(\Omega)}^p, \end{aligned} \tag{2.3}$$

where we have used the periodicity of z in Ω to deduce that the contribution from the terms centred at $x+R$ and $x-R$ are identical. This proves (2.1). Taking the p th roots of both sides followed by the supremum over $t \in (0, T)$ yields (2.2). \square

Remark 2.3. The same L^p -type estimate holds for the Gaussian and exponential detection functions (1.5)–(1.6). These cases are more straightforward since the kernels themselves are appropriately differentiable and bounded. In fact, such a condition holds for kernels of Bounded Variation, see [42, Hypothesis (H2)] and the subsequent discussion. We omit further details here.

Next, we obtain $L^p(\Omega)$ bounds on a function $k(x, t)$ when k solves a linear, first-order differential equation for each $x \in \Omega$.

Lemma 2.4. Let $0 \leq w(x, t) \in C^{1,1}(\bar{Q}_T) \cap L^{1,1}(Q_T)$ be periodic in Ω for all $t \in (0, T)$ and assume $1 < p \leq \infty$. For each $x \in \Omega$, let $k(x, \cdot)$ solve the ordinary differential equation

$$\frac{dk}{dt} = g_1(w) - g_2(w)k \tag{2.4}$$

where $g_1, g_2 \in C^1(\mathbb{R}^+)$ are nonnegative and $k(x, 0) = k_0(x) \in W^{1,2}(\Omega)$. Then, if there exists $M > 0$ such that

$$g_1(z) \leq M g_2(z) \quad \text{for all } z \geq 0, \quad (2.5)$$

there holds

$$\sup_{t \in [0, T]} \|k(\cdot, t)\|_{L^\infty(\Omega)} \leq M + \|k_0\|_{L^\infty(\Omega)} \quad (2.6)$$

Proof. First, note that by solving the differential equation directly, $k(x, \cdot) \in C^1([0, T])$. By the smoothness of $g_i(\cdot)$, $i = 1, 2$ and the boundedness of $w(x, t)$ in Q_T , $k(\cdot, t) \in L^p(\Omega)$ for any $p > 1$, for all $t \in (0, T)$. Taking the time derivative of $\frac{1}{p} \|k(\cdot, t)\|_{L^p(\Omega)}^p$ gives

$$\frac{1}{p} \frac{d}{dt} \int_{\Omega} k^p dx = \int_{\Omega} k^{p-1} g_1(w) dx - \int_{\Omega} k^p g_2(w) dx. \quad (2.7)$$

We now apply Young's inequality. To this end, we carefully rewrite it as

$$\begin{aligned} k^{p-1} g_1(w) &= k^{p-1} g_2(w)^{(p-1)/p} \cdot \frac{g_1(w)}{g_2(w)^{(p-1)/p}} \\ &\leq \frac{1}{p_1} (k^{p-1} g_2(w)^{(p-1)/p})^{p_1} + \frac{1}{q_1} \left(\frac{g_1(w)}{g_2(w)^{(p-1)/p}} \right)^{q_1}, \end{aligned} \quad (2.8)$$

where $p_1, q_1 > 1$ satisfy $p_1^{-1} + q_1^{-1} = 1$. Choosing $p_1 = p/(p-1)$ and $q_1 = p$, Eq. (2.7) then becomes

$$\frac{d}{dt} \int_{\Omega} k^p dx \leq \int_{\Omega} \left(\frac{g_1(w)}{g_2(w)} \right)^p g_2(w) dx \quad (2.9)$$

Using bound (2.5) we then have

$$\frac{d}{dt} \int_{\Omega} k^p dx \leq M^p \|g_2(w(\cdot, t))\|_{L^1(\Omega)}. \quad (2.10)$$

Integrating both sides from 0 to t yields

$$\|k(\cdot, t)\|_{L^p(\Omega)}^p \leq M^p \|g_2(w)\|_{L^{1,1}(Q_T)} + \|k_0\|_{L^p(\Omega)}^p. \quad (2.11)$$

Taking p th roots of both sides and sending $p \rightarrow \infty$ leaves

$$\|k(\cdot, t)\|_{L^\infty(\Omega)} \leq M + \|k_0\|_{L^\infty(\Omega)}. \quad (2.12)$$

Taking the supremum over $t \in (0, T)$ yields (2.6), completing the proof. \square

We also highlight the following properties of $k(x, t)$ inherited by the function $w(x, t)$, a simple consequence of solving the ordinary differential equation.

Proposition 2.5. Suppose $k(x, \cdot)$ solves (2.4) with $w \in C^{1,1}(\overline{Q_T})$ periodic in Ω . Then, $k(x, t) \in C^{1,2}(\overline{Q_T})$. Moreover, $k(\cdot, t)$ is periodic in Ω for all $t > 0$.

Finally, we obtain L^p estimates on the time/space derivatives k_t and k_x .

Theorem 2.6. Assume the same conditions as in Lemma 2.4 hold. Assume also that there exists $N > 0$ and $q \geq 1$ fixed so that

$$g_2(z) \leq N(1 + z^q) \quad \text{for all } z \geq 0. \quad (2.13)$$

Assume in addition that $w_x \in L^{2,2}(Q_T)$ and $\sup_{t \in (0, T)} \|w(\cdot, t)\|_{L^p(\Omega)} < \infty$ for all $p \geq 1$. Then there holds

$$\begin{aligned} \sup_{t \in (0, T)} \|k_t(\cdot, t)\|_{L^p(\Omega)} \leq \\ 4N \left(M + \sup_{t \in (0, T)} \|k(\cdot, t)\|_{L^\infty(\Omega)} \right) \left(|\Omega|^{1/p} + \sup_{t \in (0, T)} \|w(\cdot, t)\|_{L^{pq}(\Omega)}^q \right) \end{aligned} \quad (2.14)$$

for any $p \in (1, \infty)$. Moreover, if for some $\tilde{N} > 0$, $\tilde{q} \geq 0$ fixed we have that

$$\left| g_1'(z) \right|, \left| g_2'(z) \right| \leq \tilde{N}(1 + z^{\tilde{q}}) \quad \text{for all } z \geq 0, \quad (2.15)$$

then there exists a constant $C > 0$ depending only on T , \tilde{N} , and \tilde{q} so that

$$\begin{aligned} \sup_{t \in (0, T)} \|k_x(\cdot, t)\|_{L^p(\Omega)} \leq C \sup_{t \in (0, T)} \|(1 + w^{\tilde{q}})(\cdot, t)\|_{L^{2p/(2-p)}(\Omega)} \|w_x\|_{L^{2,2}(Q_T)} \\ + \|(k_0)_x\|_{L^p(\Omega)}, \end{aligned} \quad (2.16)$$

for any $p \in (1, 2)$ whenever $\tilde{q} > 0$, and any $p \in (1, 2]$ whenever $\tilde{q} = 0$.

Proof. Integrating $|k_t|^p$ over Ω , applying an elementary inequality, and using (2.5) yields

$$\begin{aligned} \int_{\Omega} |k_t|^p dx &= \int_{\Omega} |g_1(w) - g_2(w)k|^p dx \\ &\leq 2^{p-1} \int_{\Omega} (|g_1(w)|^p + |g_2(w)|^p |k|^p) dx \\ &\leq 2^{p-1} \int_{\Omega} (M^p + |k|^p) |g_2(w)|^p dx \end{aligned} \quad (2.17)$$

Estimating further, we use the bound on k along with bound (2.13) and the same elementary inequality to see that

$$\begin{aligned} \int_{\Omega} |k_t|^p dx &\leq 2^{p-1} (M^p + \|k(\cdot, t)\|_{L^\infty(\Omega)}^p) \int_{\Omega} |g_2(w)|^p dx \\ &\leq 4^{p-1} N^p (M^p + \|k(\cdot, t)\|_{L^\infty(\Omega)}^p) \int_{\Omega} (1 + w^{pq}) dx \\ &\leq 4^p N^p (M^p + \|k(\cdot, t)\|_{L^\infty(\Omega)}^p) (|\Omega| + \|w(\cdot, t)\|_{L^{pq}(\Omega)}^{pq}). \end{aligned}$$

Thus, we take the p th roots of both sides followed by the supremum over $t \in (0, T)$ to obtain (2.14). This completes the first part of the proof.

Next, we obtain L^p bounds on k_x for any $p \in (1, 2)$. Solving the ordinary differential equation, we may compute $k_x(x, t)$ as follows:

$$\begin{aligned} k_x(x, t) &= \frac{\partial}{\partial x} \left(\int_0^t e^{-\int_s^t g_2(w) d\xi} g_1(w) ds + k_0(x) \right) \\ &= \int_0^t e^{-\int_s^t g_2(w) d\xi} \left(g_1'(w) w_x - \int_s^t g_2'(w) w_x d\xi \right) ds + (k_0)_x. \end{aligned} \quad (2.18)$$

Therefore, estimating crudely and using bound (2.15), there holds

$$\begin{aligned} |k_x| &\leq \int_0^T \left(|g_1'(w)| |w_x| + \int_0^T |g_2'(w)| |w_x| d\xi \right) ds + |(k_0)_x| \\ &\leq \int_0^T (|g_1'(w)| + T |g_2'(w)|) |w_x| ds + |(k_0)_x| \\ &\leq \tilde{N}(1 + T) \int_0^T (1 + w^{\tilde{q}}) |w_x| ds + |(k_0)_x|. \end{aligned} \quad (2.19)$$

Raising both sides to the power p , integrating over Ω and estimating via an elementary application of Hölder's inequality in the temporal domain yields

$$\begin{aligned} \int_{\Omega} |k_x|^p dx &\leq \tilde{N}^p (1 + T)^p \int_{\Omega} \left(\int_0^T (1 + w^{\tilde{q}}) |w_x| ds \right)^p dx + \|(k_0)_x\|_{L^p(\Omega)}^p \\ &\leq \tilde{N}^p (1 + T)^p T^{p-1} \iint_{Q_T} (1 + w^{\tilde{q}})^p |w_x|^p dx ds + \|(k_0)_x\|_{L^p(\Omega)}^p. \end{aligned} \quad (2.20)$$

We now apply Hölder's inequality in the spatial domain as follows:

$$\int_{\Omega} (1 + w^{\tilde{q}})^p |w_x|^p dx \leq \left(\int_{\Omega} |w_x|^{pp_1} dx \right)^{1/p_1} \left(\int_{\Omega} (1 + w^{\tilde{q}})^{pq_1} dx \right)^{1/q_1},$$

where we again choose $p_1 = 2/p > 1$ so that $q_1 = 2/(2-p) > 1$. Simplifying and taking the supremum over $t \in (0, T)$ for the lower order term, we find

$$\int_{\Omega} (1 + w^{\tilde{q}})^p |w_x|^p dx \leq \|w_x(\cdot, t)\|_{L^2(\Omega)}^p \sup_{t \in (0, T)} \|(1 + w^{\tilde{q}})(\cdot, t)\|_{L^{2p/(2-p)}(\Omega)}^p$$

(2.20) then becomes

$$\begin{aligned} \int_{\Omega} |k_x|^p dx &\leq \tilde{N}^p (1 + T)^p T^{p-1} \sup_{t \in (0, T)} \|(1 + w^{\tilde{q}})(\cdot, t)\|_{L^{2p/(2-p)}(\Omega)}^p \\ &\quad \times \int_0^T \|w_x(\cdot, s)\|_{L^2(\Omega)}^p ds \end{aligned}$$

$$+ \|(k_0)_x\|_{L^p(\Omega)}. \tag{2.21}$$

Finally, we apply Hölder's inequality in the temporal domain once more as follows:

$$\int_0^T \|w_x(\cdot, s)\|_{L^2(\Omega)}^p ds \leq T^{1-p/2} \|w_x\|_{L^{2,2}(Q_T)}^p,$$

whence (2.21) becomes

$$\int_{\Omega} |k_x|^p dx \leq \tilde{N}^p (1+T)^p T^{p/2} \sup_{t \in (0,T)} \|(1+w^{\tilde{q}})(\cdot, t)\|_{L^{2p/(2-p)}(\Omega)}^p \|w_x\|_{L^{2,2}(Q_T)}^p + \|(k_0)_x\|_{L^p(\Omega)}^p. \tag{2.22}$$

Taking the p th roots of both sides followed by the supremum over $t \in (0, T)$ yields (2.16), valid for any $p \in (1, 2)$. Finally, if $\tilde{q} = 0$, the dependence on $w^{\tilde{q}}$ vanishes and the bound holds for $p = 2$, completing the proof. \square

2.2. Existence & uniqueness

We are now prepared to use these preliminary estimates to prove the existence of a weak solution. Much of the heavy lifting is now complete. What remains is to construct an appropriate sequence of approximate solutions and use our previously obtained estimates to extract a convergent subsequence.

Proof of Theorem 1.1. We prove the existence of a global weak solution to the following general system subject to periodic boundary conditions:

$$\begin{cases} u_t = du_{xx} + \alpha(u\bar{k}_x)_x + f(u), & \text{in } Q_T, \\ k_t = g_1(u) - g_2(u)k & \text{in } Q_T, \end{cases} \tag{2.23}$$

where systems (1.8.a) and (1.8.b) are obtained by choosing $g_1(u) := g(u)$, $g_2(u) := \mu + \beta u$ or $g_1(u) := \kappa g(u)$, $g_2(u) := \mu + \beta u + g(u)$, respectively.

First, we construct a sequence of approximate solutions via the following iteration scheme:

$$\begin{cases} (u_n)_t = d(u_n)_{xx} + \alpha(u_n(\bar{k}_n)_x) + f(u_n), & \text{in } Q_T, \\ (k_n)_t = g_1(u_{n-1}) - g_2(u_{n-1})k_n & \text{in } Q_T, \end{cases} \tag{2.24}$$

for $n \geq 2$, where we choose $(u_n(x, 0), k_n(x, 0)) = (u_0(x), k_0(x))$ for each n . Note carefully that $u_n = u_n(x, t)$ is a function defined in $\overline{Q_T}$ for all $n \geq 1$, whereas $u_0 = u_0(x)$ denotes the fixed initial data of the original problem. The same holds for $\{k_n\}_{n \geq 2}$, each of which is defined over $\overline{Q_T}$; notice also that we do not refer to $k_1(x, t)$ as we require only $u_1(x, t)$ to initiate.

Through this construction, we generate a sequence of solutions $\{(u_n, k_n)\}_{n \geq 2}$. More precisely, we choose the initial iterate $0 < u_1(x, t) \in C^{2+\sigma, 1+\sigma/2}(Q_T)$ for some $\sigma \in (0, 1)$. By solving differential equation for $k_2(x, t)$, the dependence of $k_2(x, t)$ on the sufficiently regular functions $u_1(x, t)$ and $g_i(\cdot)$, $i = 1, 2$, ensures that $k_2 \in C^{2+\sigma, 1+\sigma/2}(\overline{Q_T})$ for some (possibly smaller) $\sigma \in (0, 1)$ as well. Furthermore, the positivity of u_1 and $u_1(x, 0) = u_0(x)$ ensures that $k_2 \geq 0$ in Q_T . Then, the existence of a nonnegative, nontrivial solution $u_2(x, t) \in C^{2+\sigma, 1+\sigma/2}(\overline{Q_T})$ follows from the classical theory of parabolic equations since it is a second order, semi-linear parabolic equation with Hölder continuous coefficients, see., e.g., [45, Theorems 5.1-5.3] (note that nonnegativity follows from Harnack's inequality [46, Theorems 8.1.1-8.1.3]). Therefore, there exists a nonnegative, nontrivial classical solution pair (u_2, k_2) each belonging to $C^{2+\sigma, 1+\sigma/2}(\overline{Q_T})$ for some $\sigma \in (0, 1)$. One may then proceed inductively, proving the existence of a nonnegative, nontrivial classical solution pair (u_n, k_n) for any $n \geq 3$ using the regularity of the previous iterate $u_{n-1}(x, t)$. We now seek uniform bounds in a weaker setting.

To this end, fix $n \geq 2$. It is easy to obtain L^1 -bounds on u_n as follows:

$$\frac{d}{dt} \int_{\Omega} u_n dx = \int_{\Omega} f(u_n) dx \leq f'(0) \int_{\Omega} u_n dx, \tag{2.25}$$

where we have integrated by parts, applied the boundary conditions, and used the assumed bound $f(z) \leq f'(0)z$ for all $z \geq 0$. Grönwall's inequality implies that

$$\|u_n(\cdot, t)\|_{L^1(\Omega)} \leq e^{f'(0)T} \|u_0\|_{L^1(\Omega)}.$$

Thus, integrating over $(0, T)$ yields

$$\|u_n\|_{L^{1,1}(Q_T)} \leq T e^{f'(0)T} \|u_0\|_{L^1(\Omega)}, \tag{2.26}$$

and so $\{u_n\}_{n \geq 1}$ is uniformly bounded in $L^{1,1}(Q_T)$ for any $T > 0$ fixed.

Return now to the equation for k_n . The smoothness of the iterates u_n allows us to apply Lemma 2.4, giving us

$$\sup_{t \in (0,T)} \|k_n(\cdot, t)\|_{L^\infty(\Omega)} \leq M + \|k_0\|_{L^\infty(\Omega)}. \tag{2.27}$$

Note that $k_0 \in W^{1,2}(\Omega) \Rightarrow k_0 \in L^\infty(\Omega)$ by the Sobolev embedding. Then, Lemma 2.1 paired with estimate (2.27) implies that

$$\begin{aligned} \sup_{t \in (0,T)} \|(\bar{k}_n)_x(\cdot, t)\|_{L^\infty(\Omega)} &\leq (2RL)^{-1} \sup_{t \in (0,T)} \|k_n(\cdot, t)\|_{L^\infty(\Omega)} \\ &\leq (2RL)^{-1} (M + \|k_0\|_{L^\infty(\Omega)}) =: C_1 \end{aligned} \tag{2.28}$$

Now we seek L^p -bounds on the iterates u_n . Fix $p \geq 2$. Taking the time derivative of $\frac{1}{p} \|u_n(\cdot, t)\|_{L^p(\Omega)}^p$, integrating by parts yields and using the bound for $f(\cdot)$ yields

$$\begin{aligned} \frac{1}{p} \frac{d}{dt} \int_{\Omega} u_n^p dx &= \int_{\Omega} u_n^{p-1} (d(u_n)_x + \alpha u_n (\bar{k}_n)_x) dx + \int_{\Omega} u_n^{p-1} f(u_n) dx \\ &\leq f'(0) \int_{\Omega} u_n^p dx - d(p-1) \int_{\Omega} u_n^{p-2} |(u_n)_x|^2 dx \\ &\quad + |\alpha| (p-1) \int_{\Omega} u_n^{p-1} |(u_n)_x| |(\bar{k}_n)_x| dx. \end{aligned} \tag{2.29}$$

We now use (2.28) and Cauchy's inequality with epsilon to control the third term by the second term on the right-hand side of (2.29). To this end, we estimate

$$\begin{aligned} |\alpha| u_n^{p-1} |(u_n)_x| |(\bar{k}_n)_x| &\leq |\alpha| C_1 u_n^{(p-2)/2} |(u_n)_x| |u_n|^{p/2} \\ &\leq |\alpha| C_1 \left(\frac{\epsilon}{2} u_n^p + \frac{1}{2\epsilon} u_n^{p-2} |(u_n)_x|^2 \right), \end{aligned} \tag{2.30}$$

where we choose $\epsilon = d^{-1} |\alpha| C_1$. Paired with (2.29), this leaves

$$\begin{aligned} \frac{1}{p} \frac{d}{dt} \int_{\Omega} u_n^p dx &\leq -\frac{d}{2} \int_{\Omega} u_n^{p-2} |(u_n)_x|^2 dx \\ &\quad + (f'(0) + C_1^2 \alpha^2 d^{-1} (p-1)) \int_{\Omega} u_n^p dx \end{aligned} \tag{2.31}$$

Therefore, dropping the negative term and applying Grönwall's inequality yields

$$\|u_n(\cdot, t)\|_{L^p(\Omega)}^p \leq e^{(f'(0) + C_1^2 \alpha^2 d^{-1} (p-1))T} \|u_0\|_{L^p(\Omega)}^p.$$

Taking p th roots followed by the supremum over $t \in (0, T)$ yields the estimate

$$\begin{aligned} \sup_{t \in (0,T)} \|u_n(\cdot, t)\|_{L^p(\Omega)} &\leq e^{(f'(0) + C_1^2 \alpha^2 d^{-1} (p-1))T} \|u_0\|_{L^p(\Omega)} \\ &=: C_2, \end{aligned} \tag{2.32}$$

noting that the exponent depends critically on p . Next, we return to (2.31) for the case $p = 2$. Upon rearrangement, we apply estimate (2.32) to obtain

$$\begin{aligned} \frac{1}{2} \frac{d}{dt} \int_{\Omega} u_n^2 dx + \frac{d}{2} \int_{\Omega} |(u_n)_x|^2 dx &\leq (f'(0) + C_1^2 \alpha^2 d^{-1}) \int_{\Omega} u_n^2 dx \\ &\leq C_2^2 (f'(0) + C_1^2 \alpha^2 d^{-1}) \\ &=: C_3. \end{aligned} \tag{2.33}$$

Integrating both sides from 0 to T yields

$$\frac{1}{2} (\|u_n(\cdot, T)\|_{L^2(\Omega)}^2 - \|u_0\|_{L^2(\Omega)}^2 + d \| (u_n)_x \|^2_{L^{2,2}(Q_T)}) \leq C_3 T. \tag{2.34}$$

Ignoring the positive term on the left-hand side, we extract the desired estimate for $(u_n)_x$:

$$\|(u_n)_x\|_{L^{2,2}(Q_T)}^2 \leq d^{-1} (2C_3T + \|u_0\|_{L^2(\Omega)}) =: C_4^2. \quad (2.35)$$

We now immediately have the boundedness of $(k_n)_x$ and $(k_n)_t$ for any $n \geq 2$ in some L^p spaces. Indeed, by [Theorem 2.6](#), estimates [\(2.27\)](#), [\(2.32\)](#) and [\(2.35\)](#) imply the existence of a constant C_5 , independent of n , such that

$$\sup_{t \in (0,T)} \|(k_n)_t(\cdot, t)\|_{L^p(\Omega)}, \quad \sup_{t \in (0,T)} \|(k_n)_x(\cdot, t)\|_{L^p(\Omega)} \leq C_5, \quad (2.36)$$

for any $p \in (1, 2)$.

We now appeal to standard L^p -estimates for parabolic equations and the Sobolev embedding to improve our estimates on u_n . If we expand the equation for u_n it reads

$$(u_n)_t - d(u_n)_{xx} = \alpha \left(\overline{(k_n)_x} (u_n)_x + u_n \overline{(k_n)_{xx}} \right) + f(u_n).$$

Obviously, $f(z) \leq f'(0)z$ and $u_n \in L^{p,p}(Q_T)$ for any $p \geq 1$ gives us that $f(u_n) \in L^{p,p}(Q_T)$ as well. Then, L^p -estimates for strong solutions (see, e.g., [\[47\]](#)) ensures that there holds

$$\|u_n\|_{W_r^{2,1}(Q_T)} \leq C \left(\left\| \overline{(k_n)_x} (u_n)_x \right\|_{L^r(Q_T)} + \left\| u_n \overline{(k_n)_{xx}} \right\|_{L^r(Q_T)} + \|u_n\|_{L^r(Q_T)} \right), \quad (2.37)$$

for some $C > 0$, for any $r > 1$. Choosing $r \in (1, p)$, Hölder's inequality gives

$$\|u_n \overline{(k_n)_{xx}}\|_{L^r(Q_T)} \leq \|u_n\|_{L^{pr/(p-r)}(Q_T)} \left\| \overline{(k_n)_{xx}} \right\|_{L^p(Q_T)}. \quad (2.38)$$

By [Lemma 2.1](#), the bound [\(2.32\)](#) and [\(2.36\)](#), we may further estimate as

$$\begin{aligned} \|u_n\|_{L^{pr/(p-r)}(Q_T)} \left\| \overline{(k_n)_{xx}} \right\|_{L^p(Q_T)} &\leq (2RL)^{-1} C_2 \sup_{t \in (0,T)} \|(k_n)_x(\cdot, t)\|_{L^p(\Omega)} \\ &\leq (2RL)^{-1} C_2 C_5 =: C_6, \end{aligned} \quad (2.39)$$

for any $r \in (1, p)$, where C_6 does not depend on n . Similarly, there holds

$$\left\| \overline{(k_n)_x} (u_n)_x \right\|_{L^r(Q_T)} \leq C_7,$$

where C_7 does not depend on n . Hence,

$$\|u_n\|_{W_r^{2,1}(Q_T)} \leq C(C_2 + C_5 + C_6),$$

and so $\{u_n\}_{n \geq 2}$ is bounded in $W_r^{2,1}(Q_T)$ for any $r \in (1, p)$. Since p can be chosen as close to 2 as we like, we choose $r \in (\frac{3}{2}, 2)$ and apply the Sobolev embedding to conclude that in fact

$$\|u_n\|_{C^{\sigma,\sigma/2}(\overline{Q_T})} \leq \tilde{C} \|u_n\|_{W_r^{2,1}(Q_T)} \leq \tilde{C} C(C_2 + C_5 + C_6), \quad (2.40)$$

for any $\sigma \in (0, \frac{1}{2})$, for some $\tilde{C} > 0$. In particular, u_n is uniformly bounded in $\overline{Q_T}$, independent of n .

We are now ready to obtain bounds on the time derivative $(u_n)_t$. While the previous step gives L^p -bounds on the time derivative for $p \in (1, 2)$ only, with a bit of extra effort we can show that it also holds for $p = 2$. These estimates follow from standard arguments used in the development of the L^2 -theory of parabolic equations (see, e.g., [\[48, Ch. 3.3\]](#)), using all previous bounds. We show the key details only.

First, note that bound [\(2.16\)](#) in [Theorem 2.6](#) paired with the uniform boundedness of the iterates $\{u_n\}_{n \geq 2}$ over $\overline{Q_T}$ obtained in [\(2.40\)](#) implies that in fact $\{(k_n)_x\}_{n \geq 2}$ is uniformly bounded in $L^{2,2}(Q_T)$. Multiplying the equation for u_n by $(u_n)_t$ and integrating over Ω gives

$$\int_{\Omega} |(u_n)_t|^2 dx = \int_{\Omega} (u_n)_t \left(d(u_n)_{xx} + \alpha u_n \overline{(k_n)_x} + f(u_n) \right) dx \quad (2.41)$$

By the regularity of the iterates (u_n, k_n) for fixed n , we may exchange the order of differentiation and integrate by parts to obtain

$$\int_{\Omega} |(u_n)_t|^2 dx = -\frac{d}{2} \int_{\Omega} \left(|(u_n)_x|^2 \right)_t dx + \int_{\Omega} (u_n)_t f(u_n) dx$$

$$+ \alpha \int_{\Omega} (u_n)_t \left((u_n)_x \overline{(k_n)_x} + u_n \overline{(k_n)_{xx}} \right) dx. \quad (2.42)$$

Integrating from 0 to T and dropping the negative term, we are left with

$$\begin{aligned} \iint_{Q_T} |(u_n)_t|^2 dx dt &\leq \frac{d}{2} \|(u_0)_x\|_{L^2(\Omega)}^2 + \iint_{Q_T} (u_n)_t f(u_n) dx \\ &+ \alpha \iint_{Q_T} (u_n)_t \left((u_n)_x \overline{(k_n)_x} + u_n \overline{(k_n)_{xx}} \right) dx. \end{aligned} \quad (2.43)$$

We then estimate crudely as follows: since u_n and $\overline{(k_n)_x}$ are uniformly bounded in $\overline{Q_T}$ by [\(2.28\)](#) and [\(2.40\)](#), and since $(u_n)_x$ and $\overline{(k_n)_{xx}}$ are uniformly bounded in $L^{2,2}(Q_T)$ by [\(2.35\)](#) and preceding arguments, $f(u_n)$, $(u_n)_x \overline{(k_n)_x}$ and $u_n \overline{(k_n)_{xx}}$ are all uniformly bounded in $L^{2,2}(Q_T)$. Hence, a simple application of Cauchy's inequality with epsilon yields the existence of a constant $\tilde{C}' > 0$, independent of n , such that

$$\frac{1}{2} \iint_{Q_T} |(u_n)_t|^2 dx dt \leq \frac{d}{2} \|(u_0)_x\|_{L^2(\Omega)}^2 + \tilde{C}'. \quad (2.44)$$

We now summarize the uniform estimates we have obtained and complete the limiting process.

$$\begin{aligned} u_n &\in L^\infty(0, T; L^p(\Omega)) \cap C^{\sigma,\sigma/2}(\overline{Q_T}), \\ (u_n)_x &\in L^2(0, T; L^2(\Omega)), \quad (u_n)_t \in L^2(0, T; L^2(\Omega)), \\ k_n &\in L^\infty(0, T; L^\infty(\Omega)) \cap C^{\sigma,\sigma/2}(\overline{Q_T}), \\ (k_n)_x &\in L^2(0, T; L^2(\Omega)), \quad (k_n)_t \in L^2(0, T; L^2(\Omega)). \end{aligned} \quad (2.45)$$

Hence, there exists a limit function (u_∞, k_∞) so that for any $1 \leq p \leq \infty$ and any $0 < \sigma' < \sigma < 1/2$, there holds

$$\begin{aligned} u_n &\rightarrow u_\infty, \quad k_n \rightarrow k_\infty \quad \text{strongly in } L^{p,p}(Q_T) \cap C^{\sigma',\sigma'/2}(\overline{Q_T}), \\ (u_n)_x &\rightarrow (u_\infty)_x \quad \text{strongly in } L^{2,2}(Q_T), \\ (u_n)_t &\rightarrow (u_\infty)_t \quad \text{weakly in } L^{2,2}(Q_T), \\ (k_n)_t &\rightarrow (k_\infty)_t, \quad (k_n)_x \rightarrow (k_\infty)_x \quad \text{weakly in } L^{2,2}(Q_T). \end{aligned} \quad (2.46)$$

It is not difficult to verify that (u_∞, k_∞) is indeed a weak solution to the original problem [\(2.23\)](#) in the sense of [\(1.10\)–\(1.11\)](#) and satisfies the initial data in the classical sense. Since u_n, k_n are nonnegative for all $n \geq 2$, we find that $0 \leq u_\infty, k_\infty$ in $\overline{Q_T}$. Furthermore, the solution u_∞ is nontrivial since $f'(0) > 0$, whence k_∞ is also nontrivial. We now write (u, k) for the solution obtained.

Uniqueness given initial data (u_0, k_0) follows from standard arguments and using the fact that u and k_x are uniformly bounded over Q_T . Indeed, if there were two solution pairs (u, k) and (\tilde{u}, \tilde{k}) satisfying the same initial data, an application of Cauchy's inequality with epsilon paired with the uniform boundedness of the solutions over Q_T , the smoothness of the functions $g_i(\cdot)$, $i = 1, 2$, $f(\cdot)$ (Lipschitz continuity is sufficient), and the linearity of the spatial convolution operation yields

$$\frac{1}{2} \frac{d}{dt} \int_{\Omega} \left((u - \tilde{u})^2 + (k - \tilde{k})^2 \right) dx \leq C \int_{\Omega} \left((u - \tilde{u})^2 + (k - \tilde{k})^2 \right) dx,$$

and so Grönwall's inequality implies that $\|(u - \tilde{u})(\cdot, t)\|_{L^2(\Omega)} = \|(k - \tilde{k})(\cdot, t)\|_{L^2(\Omega)} = 0$ for any $t \in (0, T)$, and uniqueness is proved.

Hence, for problem [\(1.8.a\)](#), there exists a unique, global weak solution in the sense of [\(1.10\)–\(1.11\)](#) so long as $g(u)$ satisfies the bound

$$g(z) \leq M(\mu + \beta z) \quad \forall z \geq 0,$$

for $\mu, \beta \geq 0$ fixed, for some $M > 0$. For problem [\(1.8.b\)](#), $g(z) \leq \mu + \beta z + g(z)$ holds trivially, and no further condition on g is required, concluding the proof. \square

3. Stability of spatially-constant steady states

3.1. Spatially-constant steady states

Under assumptions (H0)-(H2), system [\(1.8.a\)](#) has two constant steady-states $(0, 0)$ and $(1, \frac{\rho}{\mu + \beta})$. For simplicity, denote

$$h(u, k) := g(u) - (\mu + \beta u)k, \quad U_0 := (0, 0), \quad U_* := (1, \frac{\rho}{\mu + \beta}).$$

The ODE kinetic system corresponding to (1.8.a) is given by

$$\begin{cases} u' = f(u), & t > 0, \\ k' = g(u) - (\mu + \beta u)k, & t > 0. \end{cases} \quad (3.1)$$

Then the Jacobian matrices J_0 at U_0 and J_* at U_* of (3.1) are given by

$$J_0 = \begin{pmatrix} f_{u0} & 0 \\ g'(0) & -\mu \end{pmatrix}, \quad J_* = \begin{pmatrix} f_{u*} & 0 \\ h_{u*} & h_{k*} \end{pmatrix}, \quad (3.2)$$

where

$$\begin{aligned} f_{u0} &:= f'(0) > 0, & h_{u*} &:= h_u(U_*) = \frac{g'(1)(\mu + \beta) - \beta\rho}{\mu + \beta}, \\ f_{u*} &:= f'(1) < 0, & h_{k*} &:= h_k(U_*) = -(\mu + \beta) < 0. \end{aligned} \quad (3.3)$$

Let $\text{Tr}(J_*)$ denotes the trace of J_* , and let $\text{Det}(J_*)$ be the determinant of J_* . Then we have

$$\text{Tr}(J_*) = f_{u*} + h_{k*} < 0, \quad \text{Det}(J_*) = f_{u*}h_{k*} > 0. \quad (3.4)$$

Hence, U_* is a locally asymptotically stable steady state with respect to (3.1), and U_0 is linearly unstable with (3.1) and also (1.8.a).

3.2. Linear stability analysis

In Section 3.3 we will use spectral analysis to determine rigorously the regions of stability for the constant steady state. However, the formalism required for spectral analysis can obscure the central message. Therefore, it is valuable first to perform linear stability analysis of U_* with respect to spatially inhomogeneous perturbations made of basis functions of L^2_{per} . This gives a quick route to an answer for the first point at which the homogeneous state becomes unstable, which we then make rigorous via a more precise spectral analysis.

To this end, we assume that non-constant perturbations of the constant steady state have the following form at arbitrarily small times

$$\tilde{u} = u_0 e^{iq_n x + \lambda t}, \quad \tilde{k} = k_0 e^{iq_n x + \lambda t}, \quad u \approx \tilde{u} + 1, \quad k \approx \tilde{k} + \frac{\rho}{\mu + \beta}, \quad (3.5)$$

where $u_0, k_0, \lambda \in \mathbb{R}$ are constants and $q_n = \sqrt{l_n} = n\pi/L$ for $n \in \mathbb{N}$. These particular wavenumbers, q_n , are chosen as they satisfy the periodic boundary conditions. Then, neglecting nonlinear terms and applying Fourier theory, the PDEs in system (1.8.a) become

$$\lambda \begin{pmatrix} \tilde{u} \\ \tilde{k} \end{pmatrix} = M_n \begin{pmatrix} \tilde{u} \\ \tilde{k} \end{pmatrix}, \quad (3.6)$$

where

$$M_n = \begin{pmatrix} -l_n d + f'(1) & -l_n \alpha C_n(G) \\ g'(1) - \frac{\beta\rho}{\mu + \beta} & -\mu - \beta \end{pmatrix}, \quad (3.7)$$

and $C_n(G)$ (the Fourier coefficient of G) is defined in (1.12). Stability requires that the trace of M_n is negative and the determinant positive. For the determinant to be positive, we require

$$\alpha C_n(G)[g'(1)(\mu + \beta) - \beta\rho] + (\mu + \beta)^2 \left(d - \frac{f'(1)}{l_n} \right) > 0. \quad (3.8)$$

(3.8) holds when $\alpha C_n(G)$ is small or zero as $f'(1) < 0$ by (H0), and (3.8) is true for all n if α (positive or negative) is sufficiently close to 0. For the trace to be negative, we require

$$f'(1) < l_n d + \mu + \beta, \quad (3.9)$$

which is always true as the right-hand side is positive and $f'(1) < 0$ by (H0). As long as Eqs. (3.8)–(3.9) are satisfied, system (1.8.a) will be stable to perturbations of the exponential functional form given in Eq. (3.5) at wavenumber q_n . A similar process gives the analogous result for system (1.8.b), which we leave as an exercise for the reader. In the next section, we generalize this result to arbitrary perturbations for systems (1.8.a) and (1.8.b) (see Theorems 1.3 and 1.4).

3.3. Spectral analysis

We now provide a detailed spectral analysis to confirm that the insights in Section 3.2 hold. Eq. (3.6) is the eigenvalue problem to be examined here but requires further justification, which is done in Lemmas 3.3 and 3.4. This ensures that the Fourier analysis utilized is robust. Of note is the symmetry of the kernel $G(\cdot)$ about the origin, which guarantees that the coefficients $C_n(G)$ are real-valued. If G were not even, then $C_n(G)$ could be complex-valued and may lead to a Hopf bifurcation. We do not explore this direction any further in the present work. Finally, Theorem 3.6 shows other than the eigenvalues from (3.6), there exists an element belonging to the point spectrum with an infinite-dimensional kernel. In this case, it is found to be negative, and so will not affect stability. In classical reaction–diffusion systems, this does not occur, but for such coupled PDE–ODE systems, it may, and so we rule out the possibility.

The linearized equation of system (1.8.a) at a constant steady state $U_* = (u_*, k_*)$ is given by

$$\begin{cases} \tilde{u}_t = d\tilde{u}_{xx} + f_{u*}\tilde{u} + \alpha u_*(G * \tilde{k})_{xx}, & x \in (-L, L), t > 0, \\ \tilde{k}_t = h_{u*}\tilde{u} + h_{k*}\tilde{k}, & x \in (-L, L), t > 0, \\ \tilde{u}(-L, t) = \tilde{u}(L, t) = 0, & t > 0, \\ \tilde{u}_x(-L, t) = \tilde{u}_x(L, t) = 0, & t > 0. \end{cases} \quad (3.10)$$

Define the linearized operator $\mathcal{L}_*(\alpha) : X \rightarrow Y$ in (3.10) by

$$\mathcal{L}_*(\alpha) \begin{bmatrix} \phi \\ \psi \end{bmatrix} = \begin{pmatrix} d\phi_{xx} + f_{u*}\phi + \alpha u_*(G * \psi)_{xx} \\ h_{u*}\phi + h_{k*}\psi \end{pmatrix}. \quad (3.11)$$

For further spectral analysis, we first recall the following definitions and give some lemmas.

Definition 3.1 ([49, Definition 2.2.1]). Let $A : D(L) \subset X \rightarrow X$ be a linear operator on a \mathbb{K} -Banach space X with $\mathbb{K} = \mathbb{R}$ or \mathbb{C} . The resolvent set $\rho(A)$ of A is the set of all points $\lambda \in \mathbb{K}$ such that $(\lambda I - A)^{-1}$ is a bijection from $D(A)$ into X and the inverse $(\lambda I - A)^{-1}$, called the resolvent of A , is a bounded linear operator from X into itself.

Definition 3.2 ([49, Definition 4.2.1]). Let $A : D(L) \subset X \rightarrow X$ be a linear operator on a complex Banach space X . The spectrum of the operator A is defined as the complement of the resolvent set $\sigma(A) = \mathbb{C} \setminus \rho(A)$. Consider the following three conditions:

- (1) $(\lambda I - A)^{-1}$ exists;
- (2) $(\lambda I - A)^{-1}$ is bounded;
- (3) the domain of $(\lambda I - A)^{-1}$ is dense in X .

The spectrum $\sigma(A)$ can be further decomposed into three disjoint subsets.

- (a) The point spectrum is the set

$$\sigma_p(A) := \{\lambda \in \sigma(A) : \mathcal{N}(\lambda I - A) \neq \{0\}\}.$$

Elements of the point spectrum $\sigma_p(A)$ are called eigenvalues. If $\lambda \in \sigma_p(A)$, elements $x \in \mathcal{N}(\lambda I - A)$ are called eigenvectors or eigenfunctions. The dimension of $\mathcal{N}(\lambda I - A)$ is the multiplicity of λ .

- (b) The continuous spectrum is the set

$$\sigma_c(A) := \{\lambda \in \sigma(A) : (1) \text{ and } (3) \text{ hold but } (2) \text{ does not}\}.$$

- (c) The residual spectrum is the set

$$\sigma_r(A) := \{\lambda \in \sigma(A) : (\lambda I - A)^{-1} \text{ exists but } \overline{\mathcal{R}(\lambda I - A)} \neq X\}.$$

Furthermore, we have the following spectrum decomposition:

$$\sigma(A) = \sigma_p(A) \cup \sigma_c(A) \cup \sigma_r(A).$$

Lemma 3.3. Assume G satisfies (H0), and $\phi \in H^2_{per}(-L, L)$. Then

$$(G * \phi)_{xx} = G * (\phi_{xx}). \quad (3.12)$$

Proof. Assume first that G is smooth. We compute as follows:

$$\begin{aligned} (G * \phi)_{xx} &= \frac{1}{2L} \int_{-L}^L G_{xx}(x-y)\phi(y)dy = \frac{1}{2L} \int_{-L}^L G_{yy}(x-y)\phi(y)dy \\ &= \frac{1}{2L} (G_y(x+L)\phi(-L) - G_y(x-L)\phi(L) - \int_{-L}^L G_y(x-y)\phi'(y)dy) \\ &= \frac{1}{2L} (G_y(x+L)\phi(-L) - G_y(x-L)\phi(L) - G(x-L)\phi'(L) \\ &\quad + G(x+L)\phi'(-L) + \int_{-L}^L G(x-y)\phi''(y)dy) \\ &= \frac{1}{2L} (G'(x+L)\phi(-L) - G'(x-L)\phi(L) - G(x-L)\phi'(L) \\ &\quad + G(x+L)\phi'(-L)) + G * (\phi_{xx}) \\ &= G * (\phi_{xx}). \end{aligned}$$

We use symmetry of G to obtain the first line after integrating by parts so that $G_{yy}(x-y) = G_{yy}(y-x)$; periodicity ensures the boundary terms vanish in the second line. These steps are repeated in lines 3-4 to obtain the desired result. To remove the smoothness assumption on G , approximate G by G^ε through a standard mollification procedure and use Young's convolution inequality paired with the regularity of ϕ to pass the limit $\varepsilon \rightarrow 0^+$. \square

Lemma 3.4. Assume G satisfies (H0). Then

$$G * \phi_n = C_n(G)\phi_n, \quad G * \phi_{-n} = C_{-n}(G)\phi_{-n} = C_n(G)\phi_{-n} \quad (3.13)$$

where $C_n(G)$ is defined in (1.12) and ϕ_n, ϕ_{-n} are defined in (1.9).

Proof. We show the first equality only, the second being similar and using the evenness of G . For $x \in [-L, L]$,

$$\begin{aligned} G * \phi_n(x) &= \phi_n * G(x) = \frac{1}{2L} \int_{-L}^L \phi_n(x-y)G(y)dy = \frac{1}{2L} \int_{-L}^L e^{\frac{i n \pi}{L}(x-y)} G(y)dy \\ &= \frac{1}{2L} \int_{-L}^L e^{-\frac{i n \pi}{L}y} G(y)dy e^{\frac{i n \pi}{L}x} = \frac{e^{\frac{i n \pi}{L}x}}{2L} \int_{-L}^L \cos\left(\frac{n \pi}{L}y\right) G(y)dy \\ &= C_n(G)\phi_n(x). \end{aligned}$$

Note that $C_n \in \mathbb{R}$ as G is an even function from (H0). Thus the eigenspace corresponding to the eigenvalue $\lambda = C_n(G)$ is

$$V_n := \text{span} \left\{ \cos\left(\frac{n \pi}{L}x\right), \sin\left(\frac{n \pi}{L}x\right) \right\}. \quad \square \quad (3.14)$$

Following a similar approach to the proof of [35, Proposition 2.1], we obtain the following lemma.

Lemma 3.5. The spectrum of the linear operator $\mathcal{A} : D(\mathcal{A}) \subset L^2_{per}(-L, L) \rightarrow L^2_{per}(-L, L)$ defined as

$$\begin{cases} D(\mathcal{A}) = H^2_{per}(-L, L), \\ \mathcal{A}\phi = a\phi'' + b(G * \phi''), \end{cases}$$

is

$$\sigma(\mathcal{A}) = \{\mu_n = \mu_{-n} := -l_n(a + bC_n(G)), n \in \mathbb{N}_0\},$$

and the corresponding eigenfunctions are $\phi_n(x)$ and $\phi_{-n}(x)$ for $n \in \mathbb{N}_0$, where a, b are constants, and l_n, ϕ_n, ϕ_{-n} are defined in (1.9).

Now we can determine the spectral set of the linearized operator $\mathcal{L}_*(\alpha)$.

Theorem 3.6. Assume that assumptions (H0)-(H2) are satisfied. Let l_n and ϕ_n be the eigenvalues and eigenfunctions of problem (1.8). Then

$$\sigma(\mathcal{L}_*(\alpha)) = \sigma_p(\mathcal{L}_*(\alpha)) = \{\lambda_n^\pm\}_{n \in \mathbb{Z}} \cup \{h_{k^*}\}, \quad (3.15)$$

where

$$\lambda_n^\pm = \lambda_{-n}^\pm = \frac{B_n \pm \sqrt{B_n^2 - 4C_n}}{2}, \quad (3.16)$$

$$B_n = \text{Tr}(J_*) - dl_n, \quad C_n = \text{Det}(J_*) + (\alpha u_* h_{u_*} C_n(G) - dh_{k^*})l_n,$$

for $n \in \mathbb{N}_0$, and

$$\begin{aligned} (\phi_{n,\pm}, \psi_{n,\pm}) &= \left(\phi_n(x), -\frac{h_{u_*}}{h_{k^*} - \lambda_n^\pm} \phi_n(x) \right), \\ (\phi_{-n,\pm}, \psi_{-n,\pm}) &= \left(\phi_{-n}(x), -\frac{h_{u_*}}{h_{k^*} - \lambda_n^\pm} \phi_{-n}(x) \right) \end{aligned} \quad (3.17)$$

are the eigenfunctions corresponding to λ_n^\pm and λ_{-n}^\pm , where $\phi_n, \phi_{-n}, h_{u_*}, h_{k^*}, \text{Tr}(J_*), \text{Det}(J_*)$ and $C_n(G)$ are defined in (1.9), (3.3), (1.12) and (3.4), respectively. Furthermore, λ_n^\pm and λ_{-n}^\pm are eigenvalues of $\mathcal{L}_*(\alpha)$ of finite multiplicity, and h_{k^*} is an eigenvalue of infinite multiplicity.

Remark 3.7. Notice that the eigenvalues obtained from (3.16) are precisely those obtained via a linear stability analysis; different, however, is the presence of the eigenvalue h_{k^*} having infinite multiplicity. Without fully considering the entire spectrum of the operator, we cannot detect h_{k^*} .

Proof. For $\lambda \in \mathbb{C}$ and $(\xi, \eta) \in Y$, we consider the resolvent equation of $\mathcal{L}_*(\alpha)$, which is

$$\begin{cases} d\phi_{xx} + f_{u_*}\phi + \alpha u_*(G * \psi)_{xx} = \lambda\phi + \xi, \\ h_{u_*}\phi + h_{k^*}\psi = \lambda\psi + \eta, \\ \phi(-L) = \phi(L), \quad \phi'(-L) = \phi'(L). \end{cases} \quad (3.18)$$

If $\lambda \neq h_{k^*}$, from the second equation of (3.18), we have

$$\psi = \frac{\eta - h_{u_*}\phi}{h_{k^*} - \lambda}, \quad (3.19)$$

Substituting (3.19) into the first equation of (3.18) and combining with (3.12) and (3.13), we get

$$(f_{u_*} - \lambda)\phi + \left(d\phi_{xx} - \alpha u_* \frac{h_{u_*}}{h_{k^*} - \lambda} (G * \phi'') \right) = \xi. \quad (3.20)$$

Eq. (3.20) has unique solutions if and only if

$$(f_{u_*} - \lambda) \notin \sigma(\mathcal{A}) \quad (3.21)$$

holds, where \mathcal{A} is the operator defined in Lemma 3.5 with $a = d$ and $b = -\alpha u_* \frac{h_{u_*}}{h_{k^*} - \lambda}$. Then from Lemma 3.5, (3.21) is equivalent to

$$\frac{(f_{u_*} - \lambda)(h_{k^*} - \lambda)}{d(h_{k^*} - \lambda) - \alpha u_* h_{u_*} C_n(G)} \notin \{l_n\}_{n \in \mathbb{N}_0}. \quad (3.22)$$

It follows that $\mathcal{L}_*(\alpha) - \lambda I$ has a bounded inverse $(\mathcal{L}_*(\alpha) - \lambda I)^{-1}$ when (3.22) is satisfied. Otherwise, λ satisfies the following characteristic equation:

$$\lambda^2 - (\text{Tr}(J_*) - dl_n)\lambda + \text{Det}(J_*) + (\alpha u_* h_{u_*} C_n(G) - dh_{k^*})l_n = 0. \quad (3.23)$$

Therefore, $\lambda_{\pm n}^\pm$ in (3.16) are the roots of (3.23) with $\text{Re} \lambda_{\pm n}^- \leq \text{Re} \lambda_{\pm n}^+$, and (3.17) are eigenfunctions corresponding to $\lambda_{\pm n}^\pm$.

If $\lambda = h_{k^*}$, we consider

$$(\mathcal{L}_*(\alpha) - h_{k^*}I) \begin{pmatrix} \phi \\ \psi \end{pmatrix} = \begin{pmatrix} 0 \\ 0 \end{pmatrix}, \quad (3.24)$$

that is

$$\begin{cases} d\phi_{xx} + f_{u_*}\phi + \alpha u_*(G * \psi)_{xx} = h_{k^*}\phi, \\ h_{u_*}\phi = 0, \\ \phi(-L) = \phi(L), \phi'(-L) = \phi'(L). \end{cases} \quad (3.25)$$

Clearly, $\phi = 0$ and $(G * \psi)_{xx} = 0$, which imply that there exist non-zero solutions to (3.24). Then h_{k^*} is also an eigenvalue of $\mathcal{L}_*(\alpha)$, and $\dim \ker(\mathcal{L}_*(\alpha) - h_{k^*}I) = \infty$. \square

Note that $\text{Tr}(J_*) < 0, \text{Det}(J_*) > 0$ from the stability of U_* , and $l_n \geq 0$, which yields $\text{Re} \lambda_{\pm n}^- < 0$. In other words, eigenvalues h_{k^*} and $\{\lambda_{\pm n}^-\}_{n \in \mathbb{N}}$ of \mathcal{L}_* all have negative real parts, and for $n = 0$, we also have

$$\lambda_0 = \frac{\text{Tr}(J_*) + \sqrt{\text{Tr}(J_*)^2 - 4\text{Det}(J_*)}}{2} < 0.$$

On the other hand, the sign of $\lambda_{\pm n}^+$ depends on the magnitude of α . Recall α_n defined in (1.13), we immediately have the following proposition.

Proposition 3.8. Assume that assumptions (H0)-(H2) are satisfied, and $n \in \mathbb{N}$ such that $C_n(G) \neq 0$. Let $\mathcal{L}_*(\alpha)$ and α_n be defined in (1.13) and (3.11), respectively. Then 0 is an eigenvalue of $\mathcal{L}_*(\alpha)$ when $\alpha = \alpha_n$ with multiplicity of two for $n \in \mathbb{N}$, while other eigenvalues have non-zero real parts. Furthermore,

$$\mathcal{N}(\mathcal{L}_*(\alpha_n)) = \text{span} \left\{ \left(1, -\frac{h_{u^*}}{h_{k^*}} \right) \phi_n(x), \left(1, -\frac{h_{u^*}}{h_{k^*}} \right) \phi_{-n}(x) \right\}. \quad (3.26)$$

Proof. From Lemma 3.4, $C_n(G)$ is real-valued. Substituting (1.13) into (3.16) yields $\lambda_{\pm n}^+ = 0$ for $n \in \mathbb{N}$. The conclusion of eigenfunctions follows from Lemma 3.5. \square

We can now prove Theorems 1.3 and 1.4.

Proof of Theorem 1.3. From the assumptions, $h_{k^*} < 0$. We also know that $\text{Re} \lambda_{\pm n}^- < 0$. Finally for $\alpha_l < \alpha < \alpha_r$, all $\lambda_{\pm n}^+$ are negative. Hence, U_* is locally asymptotically stable with respect to (1.8.a). And when $\alpha < \alpha_l$ or $\alpha > \alpha_r$, at least one of $\lambda_{\pm n}^+$ is positive, thus U_* is unstable. \square

The proof of Theorem 1.4 is similar by repeating the same analysis. Eq. (1.8.b) has two constant steady states $\hat{U}_0 = (0, 0)$ and $\hat{U}_* = (\hat{u}_*, \hat{k}_*) = (1, \frac{\rho\kappa}{\mu+\beta+\rho})$. Let $\hat{h}(u, k) := g(u)(\kappa - k) - (\mu + \beta u)k$, we have

$$\hat{h}_{u_*} = \frac{\kappa[g'(1)(\mu + \beta) - \beta\rho]}{\mu + \beta + \rho}, \quad \hat{h}_{k_*} = -(\mu + \beta + \rho). \quad (3.27)$$

Other parts are similar to the ones for the proof of Theorem 1.3.

4. Bifurcation analysis

In this section, we prove the existence of non-constant steady-state solutions of (1.8.a) through the Bifurcation from Simple Eigenvalue Theorem [50]. From (3.26), the multiplicity of the zero eigenvalue is two, so we will restrict the solutions to even functions only to apply the bifurcation theorem.

For completeness, we first recall the abstract bifurcation theorem, the definition of K -simple eigenvalue and a perturbation result. Consider an abstract equation $F(\lambda, u) = 0$, where $F : \mathbb{R} \times X \rightarrow Y$ is a nonlinear differentiable mapping, and X, Y are Banach spaces. Crandall and Rabinowitz [50] obtained the following classical Bifurcation from Simple Eigenvalue Theorem.

Theorem 4.1 ([50, Theorem 1.17]). Suppose that $\lambda_0 \in \mathbb{R}$ and $F : \mathbb{R} \times X \rightarrow Y$ is a twice continuously differentiable mapping and that

- (i) $F(\lambda, 0) = 0$ for $\lambda \in \mathbb{R}$,
- (ii) $\dim(\mathcal{N}(F_u(\lambda_0, 0))) = \text{codim}(\mathcal{R}(F_u(\lambda_0, 0))) = 1$,
- (iii) $F_{\lambda\lambda}(\lambda_0, 0)[\phi_0] \notin \mathcal{R}(F_u(\lambda_0, 0))$ where $\mathcal{N}(F_u(\lambda_0, 0)) = \text{span}\{\phi_0\} \in X$.

Let Z be any complement of $\text{span}\{\phi_0\}$ in X , then there exist an open interval \hat{I} containing 0 and continuous functions $\lambda : \hat{I} \rightarrow \mathbb{R}$, $z : \hat{I} \rightarrow Z$, such that $\lambda(0) = \lambda_0$, $z(0) = 0$, and $u(s) = s\phi_0 + sz(s)$ satisfies $F(\lambda(s), u(s)) = 0$. Moreover, $F^{-1}(\{0\})$ near $(\lambda_0, 0)$ consists precisely of the curves $u = 0$ and the curves $\{(\lambda(s), u(s)) : s \in \hat{I}\}$.

Definition 4.2 ([51, Definition 1.2]). Let $B(X, Y)$ denote the set of bounded linear maps of X into Y , and let $T, K \in B(X, Y)$. Then $\mu \in \mathbb{R}$ is a K -simple eigenvalue of T if

$$\dim \mathcal{N}(T - \mu K) = \text{codim} \mathcal{R}(T - \mu K) = 1,$$

and if $\mathcal{N}(T - \mu K) = \text{span}\{\phi_0\}$, $K\phi_0 \notin \mathcal{R}(T - \mu K)$.

Theorem 4.3 ([51, Theorem 1.16]). Let $\{(\lambda(s), u(s)) : s \in \hat{I}\}$ be the curve of inhomogeneous solutions in Theorem 4.1. Then there exist continuously differentiable functions $r : (\lambda_0 - \varepsilon, \lambda_0 + \varepsilon) \rightarrow \mathbb{R}$, $z : (\lambda_0 - \varepsilon, \lambda_0 + \varepsilon) \rightarrow X$, $\mu : (-\delta, \delta) \rightarrow \mathbb{R}$, $w : (-\delta, \delta) \rightarrow X$, such that

$$\begin{aligned} F_u(\lambda, 0)z(\lambda) &= r(\lambda)Kz(\lambda), \quad \lambda \in (\lambda_0 - \varepsilon, \lambda_0 + \varepsilon), \\ F_u(\lambda(s), u(s, \cdot))w(s) &= \mu(s)Kw(s), \quad s \in (-\delta, \delta), \end{aligned} \quad (4.1)$$

where $r(\lambda_0) = \mu(0) = 0$, $z(\lambda_0) = w(0) = (\phi_0)$, $K : X \rightarrow Y$ is the inclusion map with $K(u) = u$. Moreover, near $s = 0$ the functions $\mu(s)$ and $-s\lambda'(s)r'(\lambda_0)$ have the same zeros and, whenever $\mu(s) \neq 0$ the same sign and satisfy

$$\lim_{s \rightarrow 0} \frac{-s\lambda'(s)r'(\lambda_0)}{\mu(s)} = 1. \quad (4.2)$$

To apply the bifurcation theorems, we define a nonlinear mapping $F : \mathbb{R} \times X \rightarrow Y$ by

$$F(\alpha, U) = \begin{pmatrix} du_{xx} + \alpha(u(G * k)_x)_x + f(u) \\ g(u) - (\mu + \beta u)k \end{pmatrix}, \quad (4.3)$$

where $U = (u, k)$, then the Frechét derivative of F at (α_n, U_*) is

$$\begin{aligned} \partial_U F(\alpha_n, U_*) \begin{pmatrix} \phi \\ \psi \end{pmatrix} &= \begin{pmatrix} d\phi_{xx} + f_{u^*}\phi + \alpha_n u^*(G * \psi)_{xx} \\ h_{u^*}\phi + h_{k^*}\psi \end{pmatrix} \\ &= \mathcal{L}_*(\alpha_n) \begin{pmatrix} \phi \\ \psi \end{pmatrix}. \end{aligned} \quad (4.4)$$

For simplicity, we denote $\mathcal{L}_*(\alpha_n)$ as \mathcal{L}_n in the following. Let

$$\begin{aligned} X^s &= \{h \in X : h(-x) = h(x), x \in (-L, L)\}, \\ Y^s &= \{h \in Y : h(-x) = h(x), x \in (-L, L)\}. \end{aligned}$$

We consider the restriction of $F : \mathbb{R} \times X^s \rightarrow Y^s$, and the restriction of $\mathcal{L}_n : X^s \rightarrow Y^s$. Denote $\mathcal{N}^s(\mathcal{L}_n)$ to be the kernel space of the operator \mathcal{L}_n in X^s , and $\mathcal{N}^s(\mathcal{L}_n^*)$ to be the kernel space of the adjoint operator \mathcal{L}_n^* in X^s . Also denote $\mathcal{R}^s(\mathcal{L}_n)$ and $\mathcal{R}^s(\mathcal{L}_n^*)$ to be the corresponding range spaces in Y^s . Then X^s and Y^s have the following decompositions:

$$\begin{aligned} X^s &= \mathcal{N}^s(\mathcal{L}_n) \oplus X_1^s, \quad Y^s = \mathcal{N}^s(\mathcal{L}_n) \oplus Y_1^s, \end{aligned} \quad (4.5)$$

where

$$\begin{aligned} \mathcal{N}^s(\mathcal{L}_n) &= \text{span} \left\{ \left(1, -\frac{h_{u^*}}{h_{k^*}} \right) \cos \left(\frac{n\pi}{L}x \right) \right\}, \\ \mathcal{N}^s(\mathcal{L}_n^*) &= \text{span} \left\{ (1, r_n) \cos \left(\frac{n\pi}{L}x \right) \right\} \text{ with } r_n = \frac{dl_n - f_{u^*}}{h_{u^*}}, \\ X_1^s &= \left\{ (h_1, h_2) \in X^s : \int_{-L}^L \left(h_1 - \frac{h_{u^*}}{h_{k^*}}h_2 \right) \cos \left(\frac{n\pi}{L}x \right) dx = 0 \right\}, \\ Y_1^s &= \mathcal{R}^s(\mathcal{L}_n) = \left\{ (h_1, h_2) \in Y^s : \int_{-L}^L (h_1 + r_n h_2) \cos \left(\frac{n\pi}{L}x \right) dx = 0 \right\}. \end{aligned}$$

Hence, $\dim(\mathcal{N}^s(\mathcal{L}_n)) = \text{codim}(\mathcal{R}^s(\mathcal{L}_n)) = 1$. We also have

$$\partial_{\alpha U} F(\alpha_n, U_*) \begin{pmatrix} \phi \\ \psi \end{pmatrix} = \begin{pmatrix} u_*(G * \psi)_{xx} \\ 0 \end{pmatrix},$$

thus

$$\begin{aligned} \partial_{\alpha U} F(\alpha_n, U_*) \left[\left(1, -\frac{h_{u^*}}{h_{k^*}} \right) \cos \left(\frac{n\pi}{L}x \right) \right]^T \\ = \left(-u_* \frac{h_{u^*}}{h_{k^*}} \frac{\partial^2}{\partial x^2} \left(G * \cos \left(\frac{n\pi}{L}x \right) \right), 0 \right)^T \notin \mathcal{R}^s(\mathcal{L}_n) \end{aligned}$$

as

$$u_* \frac{h_{u^*}}{h_{k^*}} l_n C_n(G) \int_{-L}^L \cos^2 \left(\frac{n\pi}{L}x \right) dx \neq 0,$$

as long as $C_n(G) \neq 0$. Now by applying Theorem 4.1, we obtain the existence of non-constant steady-state solutions of (1.8.a) (Theorem 1.5) and (1.8.b) (Theorem 1.6).

Near a bifurcation point $\alpha = \alpha_n$, it follows from [52] that the sign of $\alpha'_n(0)$ or the one of $\alpha''_n(0)$ when $\alpha'_n(0) = 0$ determine the bifurcation direction. If $\alpha'_n(0) \neq 0$, then a transcritical bifurcation occurs, and an inhomogeneous solution exists when $\alpha(\neq \alpha_n)$ is close to the bifurcation point α_n . If $\alpha'_n(0) = 0$ and $\alpha''_n(0) \neq 0$, then a pitchfork bifurcation occurs at $\alpha = \alpha_n$. The pitchfork bifurcation is forward if $\alpha''_n(0) > 0$ and there are two (zero) inhomogeneous solutions for $\alpha > \alpha_n$ ($\alpha < \alpha_n$), and it is backward if $\alpha''_n(0) < 0$. Since

$$\begin{aligned} & \langle \zeta, \partial_{UU} F(\alpha_n, U_*) \left[\left(1, -\frac{h_{u^*}}{h_{k^*}}\right) \cos\left(\frac{n\pi}{L}x\right) \right]^2 \rangle \\ &= \int_{-L}^L \left[\left(f_{uu^*} + r_n \left(h_{uu^*} - 2h_{uk^*} \frac{h_{u^*}}{h_{k^*}} \right) \right) \frac{1 + \cos\left(\frac{2n\pi}{L}x\right)}{2} \right. \\ & \quad \left. + 2\alpha_n l_n C_n(G) \frac{h_{u^*}}{h_{k^*}} \cos\left(\frac{2n\pi}{L}x\right) \right] \cos\left(\frac{n\pi}{L}x\right) dx = 0, \end{aligned}$$

where $f_{uu^*} \triangleq f_{uu}(U_*)$, $h_{uu^*} \triangleq h_{uu}(U_*)$, $h_{uk^*} \triangleq h_{uk}(U_*) = -\beta$, and $\zeta \in (Y^s)^*$ satisfying $N(\zeta) = \mathcal{R}^s(\mathcal{L}_n)$, then we have

$$\alpha'_n(0) = - \frac{\left\langle \zeta, \partial_{UU} F(\alpha_n, U_*) \left[\left(1, -\frac{h_{u^*}}{h_{k^*}}\right) \cos\left(\frac{n\pi}{L}x\right) \right]^2 \right\rangle}{2 \left\langle \zeta, \partial_{\alpha U} F(\alpha_n, U_*) \left[\left(1, -\frac{h_{u^*}}{h_{k^*}}\right) \cos\left(\frac{n\pi}{L}x\right) \right] \right\rangle} = 0. \quad (4.6)$$

We further calculate $\alpha''_n(0)$ as in [52],

$$\begin{aligned} \alpha''_n(0) &= - \frac{\left\langle \zeta, \partial_{UUU} F(\alpha_n, U_*) \left[\left(1, -\frac{h_{u^*}}{h_{k^*}}\right) \cos\left(\frac{n\pi}{L}x\right) \right]^3 \right\rangle}{3 \left\langle \zeta, \partial_{\alpha U} F(\alpha_n, U_*) \left[\left(1, -\frac{h_{u^*}}{h_{k^*}}\right) \cos\left(\frac{n\pi}{L}x\right) \right] \right\rangle} \\ & \quad - \frac{\left\langle \zeta, \partial_{UU} F(\alpha_n, U_*) \left[\left(1, -\frac{h_{u^*}}{h_{k^*}}\right) \cos\left(\frac{n\pi}{L}x\right), \Theta \right] \right\rangle}{\left\langle \zeta, \partial_{\alpha U} F(\alpha_n, U_*) \left[\left(1, -\frac{h_{u^*}}{h_{k^*}}\right) \cos\left(\frac{n\pi}{L}x\right) \right] \right\rangle}, \end{aligned} \quad (4.7)$$

where $\Theta = (\theta_1, \theta_2)$ is the unique solution of

$$\partial_{UU} F(\alpha_n, U_*) \left[\left(1, -\frac{h_{u^*}}{h_{k^*}}\right) \cos\left(\frac{n\pi}{L}x\right) \right]^2 + \partial_U F(\alpha_n, U_*) [\Theta] = 0, \quad (4.8)$$

and

$$\begin{aligned} & \partial_{UU} F(\alpha_n, U_*) \left[\left(1, -\frac{h_{u^*}}{h_{k^*}}\right) \cos\left(\frac{n\pi}{L}x\right) \right]^2 \\ &= \begin{pmatrix} f_{uu^*} \cos^2\left(\frac{n\pi}{L}x\right) + 2\alpha_n l_n C_n(G) \left(\frac{h_{u^*}}{h_{k^*}}\right) \left(\cos^2\left(\frac{n\pi}{L}x\right) - \sin^2\left(\frac{n\pi}{L}x\right)\right) \\ \left(h_{uu^*} + h_{kk^*} \left(\frac{h_{u^*}}{h_{k^*}}\right)^2 - 2h_{uk^*} \left(\frac{h_{u^*}}{h_{k^*}}\right) \right) \cos^2\left(\frac{n\pi}{L}x\right) \end{pmatrix}, \\ & \partial_U F(\alpha_n, U_*) [\Theta] \\ &= \begin{pmatrix} f_{u^*} \left(\theta_1^2 + \theta_2^2 \cos\left(\frac{2n\pi}{L}x\right)\right) - 4l_n \cos\left(\frac{2n\pi}{L}x\right) \left(d\theta_1^2 + \alpha_n u_n C_n(G)\theta_2^2\right) \\ h_{u^*} \left(\theta_1^2 + \theta_2^2 \cos\left(\frac{2n\pi}{L}x\right)\right) + h_{k^*} \left(\theta_1^2 + \theta_2^2 \cos\left(\frac{2n\pi}{L}x\right)\right) \end{pmatrix}. \end{aligned}$$

From [12] and 4.3, we assume $\Theta = (\theta_1, \theta_2)$ has the following form

$$\theta_1 = \theta_1^1 + \theta_1^2 \cos\left(\frac{2n\pi}{L}x\right), \quad \theta_2 = \theta_2^1 + \theta_2^2 \cos\left(\frac{2n\pi}{L}x\right). \quad (4.9)$$

Combining (4.8) and (4.9), after calculation, we have

$$\begin{aligned} \theta_1^1 &= -\frac{f_{uu^*}}{2f_{u^*}}, \quad \theta_2^1 = \frac{-(-f_{uu^*}h_{k^*}^2h_{u^*} + f_{u^*}h_{uu^*}h_{k^*}^2 - 2f_{u^*}h_{uk^*}h_{k^*}h_{u^*} + f_{u^*}h_{kk^*}h_{u^*}^2)}{2f_{u^*}h_{k^*}^3}, \\ \theta_1^2 &= \frac{-(-f_{uu^*}h_{k^*}^3 + 4C_n(G)\alpha_n l_n(h_{k^*}^2h_{u^*} + u_n h_{uu^*}h_{k^*}^2 - 2u_n h_{uk^*}h_{k^*}h_{u^*} + u_n h_{kk^*}h_{u^*}^2))}{2h_{k^*}^2(f_{u^*}h_{k^*} - 4dh_{k^*}l_n + 4C_n(G)\alpha_n u_n h_{u^*}l_n)}, \\ \theta_2^2 &= \frac{f_{uu^*}h_{k^*}^2h_{u^*} - (f_{u^*} - 4dl_n)(h_{uu^*}h_{k^*}^2 + h_{kk^*}h_{u^*}^2 - 2h_{u^*}h_{k^*}h_{uk^*}) + 4C_n(G)l_n\alpha_n h_{u^*}^2h_{k^*}}{2h_{k^*}^2(f_{u^*}h_{k^*} - 4dh_{k^*}l_n + 4C_n(G)\alpha_n u_n h_{u^*}l_n)}, \end{aligned} \quad (4.10)$$

Moreover, we can calculate

$$\begin{aligned} & \partial_{UUU} F(\alpha_n, U_*) \left[\left(1, -\frac{h_{u^*}}{h_{k^*}}\right) \cos\left(\frac{n\pi}{L}x\right) \right]^3 \\ &= \begin{pmatrix} f_{uuu^*} \cos^3\left(\frac{n\pi}{L}x\right) \\ \left(h_{uuu^*} - h_{kkk^*} \left(\frac{h_{u^*}}{h_{k^*}}\right)^3 + 3h_{ukk^*} \left(\frac{h_{u^*}}{h_{k^*}}\right) - 3h_{uuk^*} \left(\frac{h_{u^*}}{h_{k^*}}\right) \right) \cos^3\left(\frac{n\pi}{L}x\right) \end{pmatrix}, \\ & \partial_{UU} F(\alpha_n, U_*) \left[\left(1, -\frac{h_{u^*}}{h_{k^*}}\right) \cos\left(\frac{n\pi}{L}x\right), \Theta \right] = \begin{pmatrix} F_{UU1} \\ F_{UU2} \end{pmatrix}, \\ & F_{\alpha U}(\alpha_n, U_*) \left[\left(1, -\frac{h_{u^*}}{h_{k^*}}\right) \cos\left(\frac{n\pi}{L}x\right) \right] = \begin{pmatrix} u_n l_n C_n(G) \frac{h_{u^*}}{h_{k^*}} \cos\left(\frac{n\pi}{L}x\right) \\ 0 \end{pmatrix}, \end{aligned} \quad (4.11)$$

where

$$\begin{aligned} F_{UU1} &= \left(f_{uu^*} + \alpha_n l_n C_n(G) \frac{h_{u^*}}{h_{k^*}} \right) \cos\left(\frac{n\pi}{L}x\right) \left(\theta_1^1 + \theta_1^2 \cos\left(\frac{2n\pi}{L}x\right) \right) \\ & \quad + 2\alpha_n l_n C_n(G) \sin\left(\frac{n\pi}{L}x\right) \sin\left(\frac{2n\pi}{L}x\right) \left(-\frac{h_{u^*}}{h_{k^*}} \theta_1^1 + \theta_2^2 \right) \\ & \quad - 4\alpha_n l_n C_n(G) \cos\left(\frac{n\pi}{L}x\right) \cos\left(\frac{2n\pi}{L}x\right) \theta_2^2, \\ F_{UU2} &= \left(h_{uu^*} - h_{uk^*} \left(\frac{h_{u^*}}{h_{k^*}}\right) \right) \cos\left(\frac{n\pi}{L}x\right) \left(\theta_1^1 + \theta_1^2 \cos\left(\frac{2n\pi}{L}x\right) \right) \\ & \quad + \left(h_{uk^*} - h_{kk^*} \left(\frac{h_{u^*}}{h_{k^*}}\right) \right) \cos\left(\frac{n\pi}{L}x\right) \left(\theta_2^1 + \theta_2^2 \cos\left(\frac{2n\pi}{L}x\right) \right). \end{aligned}$$

Substituting (4.10) and (4.11) into (4.7), we can calculate $\alpha''(0)$. If $\alpha''_n(0) > 0$, then a forward pitchfork bifurcation occurs; and if $\alpha''_n(0) < 0$, then a backward pitchfork bifurcation occurs.

From Theorem 4.3, we obtain the stability of the nonconstant steady-state solution of problem (1.8.a) and (1.8.b) obtained in Theorems 1.5 and 1.6, respectively.

Theorem 4.4. Suppose the conditions of Theorem 1.5 are satisfied, and let $(\alpha_n(s), U(s, \cdot))$ ($|s| < \delta$) be the non-constant steady state solutions bifurcating from the constant ones at $\alpha = \alpha_n$. Then a pitchfork bifurcation occurs at $\alpha = \alpha_n$ if $\alpha''_n(0) \neq 0$.

- (i) At $\alpha = \alpha_r > 0$, suppose that $\alpha_r = \alpha_N$ for $N \in \mathbb{N}$, then the pitchfork bifurcation is forward and the bifurcating solutions are locally asymptotically stable with respect to (1.8.a) if $\alpha''_N(0) > 0$, and it is backward and the bifurcating solutions are unstable if $\alpha''_N(0) < 0$. The other bifurcating solutions near $\alpha_n > 0$ for $n \neq N$ are all unstable.
- (ii) At $\alpha = \alpha_l < 0$, suppose that $\alpha_l = \alpha_M$ for $M \in \mathbb{N}$, then the pitchfork bifurcation is backward and the bifurcating solutions are locally asymptotically stable with respect to (1.8.a) if $\alpha''_M(0) < 0$, and it is forward and the bifurcating solutions are unstable if $\alpha''_M(0) > 0$. The other bifurcating solutions near $\alpha_n < 0$ for $n \neq M$ are all unstable.

Proof. Let $r(\alpha)$ be the eigenvalue of the corresponding linearization operator for the constant solution U_* such that $r(\alpha_n) = 0$. From (4.1),

$$F_U(\alpha, U_*) [\phi(\alpha), \psi(\alpha)]^T = r(\alpha) K [\phi(\alpha), \psi(\alpha)]^T, \quad \alpha \in (\alpha_n - \epsilon, \alpha_n + \epsilon). \quad (4.12)$$

Here $K : X \rightarrow Y$ is the inclusion map $K(U) = U$. From Theorem 3.6, we thus get

$$r(\alpha) = \frac{B_n + \sqrt{B_n^2 - 4C_n}}{2},$$

where B_n and C_n are defined in (3.16). Moreover, from the definition of B_n and C_n , we obtain

$$r'(\alpha_n) = \frac{u_n h_{u^*} C_n(G) l_n}{B_n}. \quad (4.13)$$

In particular, we have $\text{sign}(r'(\alpha_n)) = \text{sign}(\alpha_n)$ from (1.13) and (4.13). From (4.6), we have $\alpha'_n(0) = 0$ for any $n \in \mathbb{N}$, and $\alpha''_n(0)$ can be calculated as in (4.7). Thus a pitchfork bifurcation occurs at $\alpha = \alpha_n$ if $\alpha''_n(0) \neq 0$.

Suppose that $\alpha_r = \alpha_N > 0$ for some $N \in \mathbb{N}$, then $r'(\alpha_N) > 0$. If $\alpha''_N(0) > 0$, then $\alpha'_N(s) > 0$ for $s \in (0, \delta)$, and $\alpha'_N(s) < 0$ for $s \in (-\delta, 0)$. From Theorem 4.3, $\text{sign}(-s\alpha'_N(s)r'(\alpha_N)) = \text{sign}(\mu(s))$, where $\mu(s)$ is the eigenvalue of the corresponding linearization operator for the bifurcating solution at $\alpha = \alpha(s)$. Thus $\mu(s) < 0$ for $0 < |s| < \delta$. Since all other eigenvalues of linearized equation at $(\alpha_n(s), U(s, \cdot))$ are negative near $\alpha = \alpha_r$, then $(\alpha_n(s), U(s, \cdot))$ is locally asymptotically stable. Similarly if $\alpha''_N(0) < 0$, then $\mu(s) > 0$ for $0 < |s| < \delta$ hence $(\alpha_n(s), U(s, \cdot))$ is unstable. The cases for bifurcation point $\alpha = \alpha_l < 0$ or $\alpha \neq \alpha_l, \alpha_r$ can be proved similarly. \square

Theorem 4.5. *Suppose the conditions of Theorem 1.6 are satisfied. Then the same results as in Theorem 4.4 hold for Eq. (1.8.b), with U_* and α_n replaced by \hat{U}_* and $\hat{\alpha}_n$.*

When the bifurcating solutions near $\alpha = \alpha_l$ or α_r are locally asymptotically stable, one can observe a small amplitude non-constant steady state solution of (1.8.a) with a prescribed wave pattern (corresponding to N or M in Theorem 4.4). When the bifurcating solutions near $\alpha = \alpha_l$ or α_r are unstable, the corresponding bifurcating branch will bend back through a saddle-node bifurcation and likely to a large amplitude non-constant steady state solution of (1.8.a) with the same prescribed wave pattern.

5. Analysis of the model with a top-hat detection function

In this section, we study some specific cases to demonstrate some of our analytical results corresponding to different growth functions $g(\cdot)$. Depending on the functional form of memory uptake $g(\cdot)$, we establish a number of monotone/nonmonotone properties of the bifurcation values $\alpha_n(R)$. For the first two examples (sublinear and linear growth, respectively), we plot the local stability curves $\alpha_l(R)$, $\alpha_r(R)$ as they depend on the perceptual radius R , a bifurcation curve demonstrating the direction and stability of the branch obtained, and a sample solution profile just beyond the critical values $\alpha_l(R)$ and $\alpha_r(R)$. For the numerical simulations we use a pseudo-spectral method with a third order, strong stability-preserving Runge–Kutta (SSPRK3) time-stepping algorithm. Trajectories are run until the approximate time derivative u_t is small in sup-norm, i.e., once $\|u_t(\cdot, T)\|_{L^\infty} \leq 10^{-15}$. Note that our computational domain chosen is $(0, 2\pi)$, equivalent to choosing $\Omega = (-\pi, \pi)$ due to translation invariance.

To this end, let $L = \pi$ and $f(u) = u(1 - u)$. In all examples, we fix $d = \mu = \beta = 1.0$ and $\rho = 5$.

We then choose the following three cases of $g(u)$ to analyse Eq. (1.8.a) and Eq. (1.8.b) with the top-hat detection function defined in :

$$(i) g(u) = \frac{2\rho u^2}{1+u^2}; \quad (ii) g(u) = \frac{2\rho u^2}{1+u}; \quad (iii) g(u) = \rho u^2.$$

It is interesting to note that for all functional forms of $g(u)$ considered above, we always find that $g'(1)(\mu + \beta) - \rho\beta > 0$, and so from Theorems 1.5–1.6, we only expect to observe solution profiles that are *in phase* in the sense that the peaks and troughs of the population density and the spatial map are aligned. However, out-of-phase solutions are possible in principle if $g(u)$ is such that $g'(1)(\mu + \beta) - \rho\beta < 0$.

As previously noted in Remark 1.2, Cases (i) and (ii) have a global weak solution for either problem (1.8.a) or (1.8.b). In Case (iii), a global weak solution is only guaranteed by Theorem 1.1 for problem (1.8.b).

5.1. Case (i) in Eq. (1.8.a)

We consider $g(u) = \frac{2\rho u^2}{1+u^2}$; f and g satisfy assumptions (H1)-(H2).

One can calculate that $(u_*, k_*) = \left(1, \frac{\rho}{\mu + \beta}\right)$ and

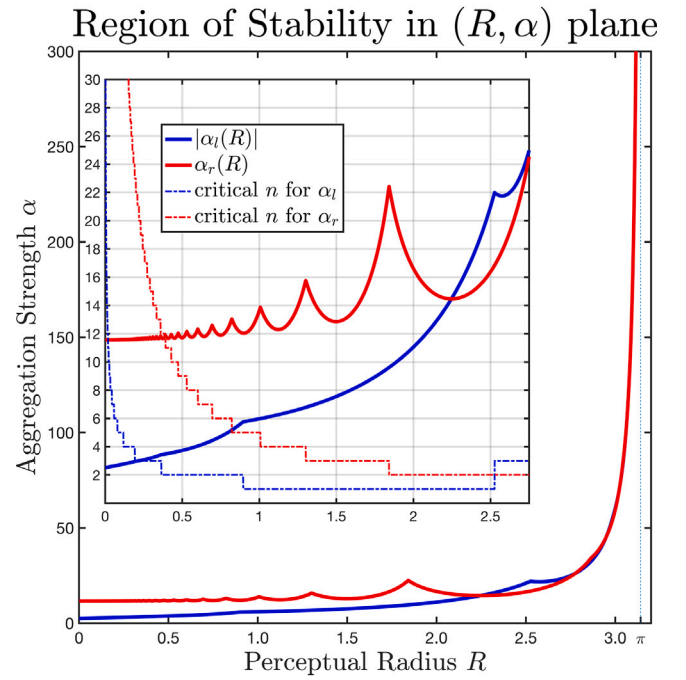


Fig. 1. The stability curves for Example (i) in Section 5.1. We display the first critical values $|\alpha_l|$ and α_r as a function of the perceptual radius R using (5.7). Under the convention of for the top-hat kernel (non-increasing from the origin), α_l corresponds to the critical attractive strength (solid blue curve) while α_r corresponds to the critical repulsive strength (solid red curve). The dashed lines represent the wavenumber at which the homogeneous state destabilizes. In the subsequent Figs. 2–3, we fix $R = 1.5$ so that the expected frequency of the bifurcating solution is $n = 1$ for attraction and $n = 3$ for repulsion.

$$\begin{aligned} f_{u*} &= -1, \quad f_{uu*} = -2, \quad f_{uuu*} = 0, \quad g_{u*} = \rho, \quad h_{u*} = \frac{\rho\mu}{\mu + \beta}, \\ h_{k*} &= -(\mu + \beta), \quad h_{uu*} = g_{uu*} = -\rho, \quad h_{uk*} = -\beta, \quad h_{kk*} = 0, \\ h_{uuu*} &= g_{uuu*} = h_{uu*} = h_{uk*} = h_{kk*} = 0. \end{aligned} \quad (5.1)$$

We consider the following model with the top-hat detection function:

$$\begin{cases} u_t = du_{xx} + \alpha(u\bar{k}_x)_x + u(1 - u), & x \in (-\pi, \pi), \quad t > 0, \\ k_t = \frac{2\rho u^2}{1+u^2} - (\mu + \beta)k, & x \in (-\pi, \pi), \quad t > 0, \end{cases} \quad (5.2)$$

subject to periodic boundary conditions, where $G(x)$ is defined as in such that $0 < R < \pi$. From (1.4), we have

$$\bar{k}(x) = \frac{1}{2\pi} \int_{x-R}^{x+R} \frac{1}{2R} k(y) dy, \quad -\pi \leq x \leq \pi, \quad (5.3)$$

and for G in , we have

$$C_n(G) = \frac{\sin(nR)}{2\pi nR}. \quad (5.4)$$

As in (3.11), the linearized operator at (α, U_*) is

$$\begin{aligned} \mathcal{L}_*(\alpha) \begin{pmatrix} \phi \\ \psi \end{pmatrix} &= \partial_U F(\alpha, U_*) \begin{pmatrix} \phi \\ \psi \end{pmatrix} \\ &= \begin{pmatrix} d\phi_{xx} - \phi + \frac{\alpha}{4RL} (\psi_x(x+R) - \psi_x(x-R)) \\ \frac{\rho\mu}{\mu + \beta} \phi - (\mu + \beta)\psi \end{pmatrix}. \end{aligned} \quad (5.5)$$

From Theorem 3.6, the spectrum of $\mathcal{L}_*(\alpha)$ is consisted of $h_{k*} = -(\mu + \beta) < 0$ and eigenvalues λ_n^\pm which satisfy the characteristic equation

$$\lambda^2 + (1 + \mu + \beta + dn^2)\lambda + (\mu + \beta) + \left(\alpha \frac{\rho\mu}{\mu + \beta} \frac{\sin(nR)}{2\pi nR} + d(\mu + \beta)\right)n^2 = 0, \quad (5.6)$$

where l_n is defined in (1.9), $n \in \mathbb{Z}$. When $n = 0$, from (3.4), all roots of (5.6) have negative real parts, hence the constant solution U_* is locally

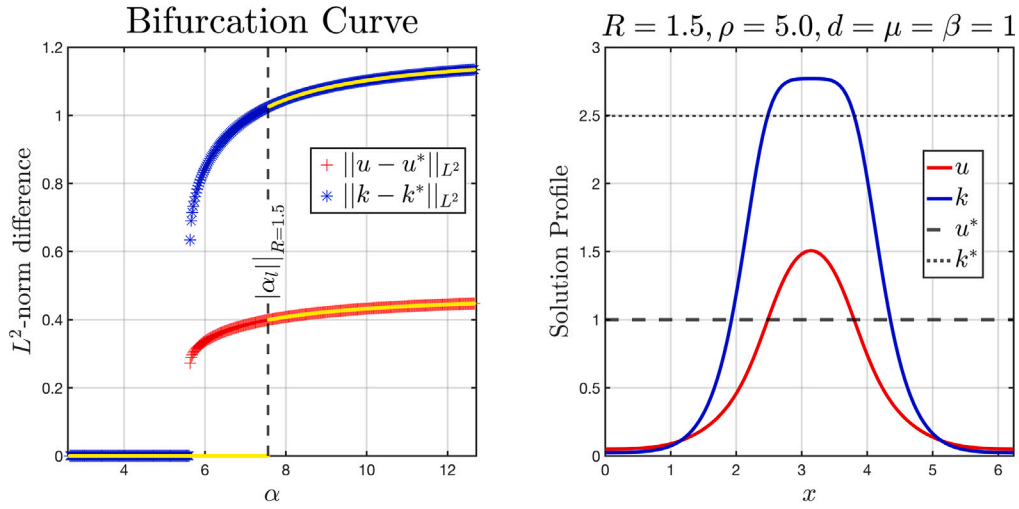


Fig. 2. The bifurcation diagram corresponding to $|\alpha_r|$ for Example (i) of Section 5 (left panel) and a sample solution profile ~ 0.1 units beyond the critical threshold $\alpha = \alpha_r(1.5)$ (right panel). (u, k) denotes a inhomogeneous stationary state, while (u^*, k^*) denotes the homogeneous state. In the left panel, the blue and red curves are obtained by first locating a spatially inhomogeneous state beyond the critical threshold α_r , and then tracing the branch forwards and backwards. As predicted by our analytical results, we observe a subcritical bifurcation with an unstable branch (not depicted) which connects with the α -axis. The yellow curves are the solution profile obtained from a small uniform perturbation (of order 10^{-3}) of the homogeneous state, demonstrating the local stability of the homogeneous state prior to the critical threshold. In the right panel, we display a solution profile of the stationary state versus the homogeneous state just beyond the critical threshold; as predicted by our analytical insights, we observe a solution profile of frequency $n = 1$; the key insight is that, since the bifurcation is subcritical, the solution profile has high-amplitude, while the low-amplitude solution is the unstable one undetectable by our time-dependent solver.

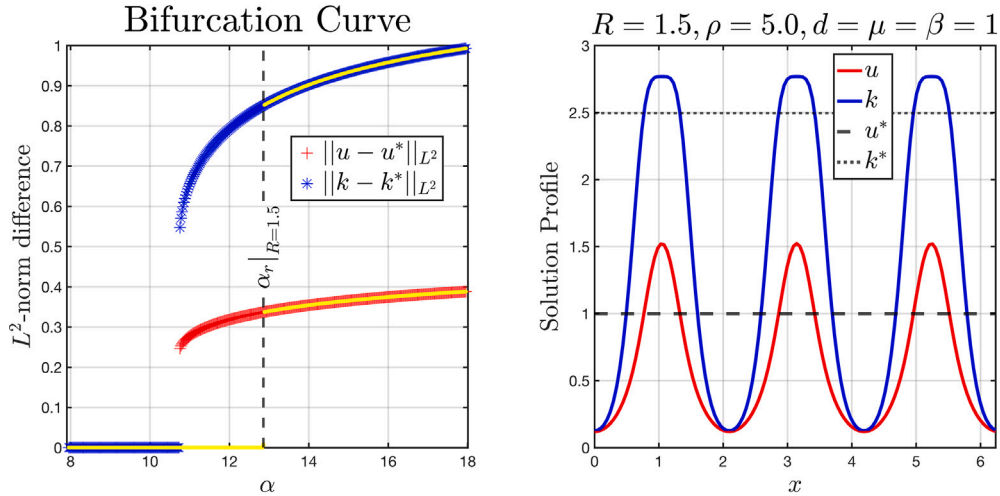


Fig. 3. The bifurcation diagram corresponding to α_r for Example (i) of Section 5 (left panel) and a sample solution profile ~ 0.1 units beyond the critical threshold $\alpha = \alpha_r(1.5)$ (right panel). The figure is almost identical to Fig. 2; the notable difference is the wavenumber at which the homogeneous state is destabilized: as predicted by our analytical results and from Fig. 1, we now have a solution profile of frequency $n = 3$, also with high amplitude.

asymptotically stable with respect to non-spatial dynamics. Note that (5.6) is an even function of n , so we consider $n \in \mathbb{N}$ below.

From (1.13), (1.14) and (5.4), we obtain

$$\begin{aligned} \alpha_n^R &= \frac{\text{Det}(J_*) - d h_{k^*} n^2}{u_* h_{u^*} n^2 \frac{\sin(nR)}{2\pi n R}} = \frac{-2\pi n R (\mu + \beta)^2}{\rho \mu \sin(nR)} \left(d + \frac{1}{n^2} \right), \\ \Sigma^+ &= \left\{ n \in \mathbb{N} : nR \in \cup_{j=0}^{\infty} (2j\pi, (2j+1)\pi) \right\}, \\ \Sigma^- &= \left\{ n \in \mathbb{N} : nR \in \cup_{j=0}^{\infty} ((2j+1)\pi, (2j+2)\pi) \right\}, \\ \alpha_l &= -\frac{2\pi(\mu + \beta)^2}{\rho \mu} \min_{n \in \Sigma^+} \frac{nR}{\sin(nR)} \left(d + \frac{1}{n^2} \right), \\ \alpha_r &= -\frac{2\pi(\mu + \beta)^2}{\rho \mu} \max_{n \in \Sigma^-} \frac{nR}{\sin(nR)} \left(d + \frac{1}{n^2} \right), \end{aligned} \quad (5.7)$$

In Fig. 1 we numerically compute the values $|\alpha_l|$ and α_r and plot them with respect to the perceptual radius R . We also display the

wavenumber at which the critical value is achieved. Now we can apply Theorems 1.3 and 1.5 to (5.2) to have the following results.

Theorem 5.1. Let $\alpha_n^R, \Sigma^+, \Sigma^-, \alpha_l, \alpha_r$ be defined in (5.7). Then the constant steady state solution $U_* = (1, \rho/(\mu + \beta))$ is locally asymptotically stable with respect to (5.2) when $\alpha_l < \alpha < \alpha_r$ and is unstable when $\alpha < \alpha_l$ or $\alpha > \alpha_r$. Moreover non-constant steady state solutions of (5.2) bifurcate from the branch of constant solutions $\Gamma_0 = \{(\alpha, U_*) : \alpha \in \mathbb{R}\}$ near $\alpha = \alpha_n^R$, and these solutions are on a curve $\Gamma_n = \{(\alpha_n(s), u_n(s, \cdot), k_n(s, \cdot)) : |s| < \delta\}$ such that $\alpha_n(0) = \alpha_n^R$ and $\alpha_n'(0) = 0$. Moreover, the following monotonicity properties hold.

- (i) Suppose $n \in \Sigma^+$ so that $\frac{\sin(nR)}{nR} > 0$. Then $\alpha_n(R) < 0$, and $\alpha_n(R)$ (in particular, α_l) is monotonically increasing with respect to ρ , is monotonically decreasing with respect to d and β , and is not monotone with respect to μ .

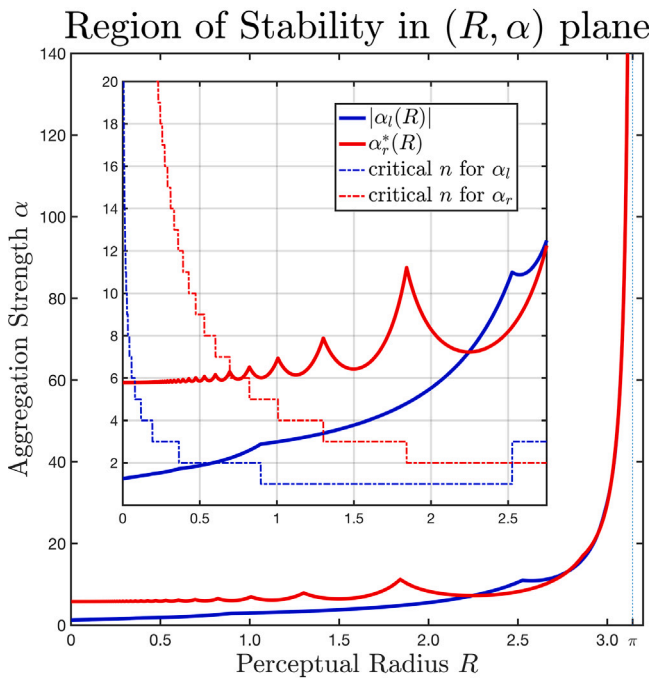


Fig. 4. The stability curves for Example (ii) in Section 5.2, obtained as in Fig. 1. We again display the first critical values $|\alpha_l|$ and α_r as a function of the perceptual radius R using (5.7). Qualitatively similar to Example (i), this case has a significantly different scale of magnitude to destabilize the homogeneous state.

(ii) Suppose $n \in \Sigma^-$ so that $\frac{\sin(nR)}{nR} < 0$. Then $\alpha_n(R) > 0$, and $\alpha_n(R)$ (in particular, α_r) is monotonically increasing with respect to d and β , is monotonically decreasing with respect to ρ , and is not monotone with respect to μ .

Using (4.7), after several calculations we find that

$$\alpha_n''(0) = \frac{(504n^4 + 645n^2 + 541)}{150C_n(G)n^2}$$

Since the numerator of the above quantity is strictly positive for all $n \geq 1$, the sign of $\alpha_n''(0)$ depends only on the sign of the Fourier coefficients of the kernel G . At α_l , we look at wavenumbers from Σ^+ and so $\text{sign}(\alpha''(0)) > 0$; by Theorem 4.4 the pitchfork bifurcation is forward, and the bifurcating solution is unstable. Similarly, at α_r , we look at wavenumbers from Σ^- and so $\text{sign}(\alpha''(0)) < 0$; by Theorem 4.4 the pitchfork bifurcation is backward and the bifurcating solution is unstable. This is precisely what is observed in Figs. 2–3, where both cases feature a high amplitude solution curve appearing before the critical thresholds $|\alpha_l|$ and α_r .

The monotonicity properties described above can be understood intuitively. In Case (i) of Theorem 5.1, we consider cases of aggregation ($\alpha < 0$), and so a decreasing behaviour requires higher rates of advection to destabilize the constant steady state, while an increasing behaviour allows for destabilization of the constant steady state at lower advection rates. As is generally understood for diffusion–advection models, diffusion has a stabilizing effect, and higher rates of diffusion, therefore, require comparably high magnitudes of advection to destabilize the constant steady state. Similarly, an increased value of β , a ‘rate of safe return’, also requires an increased magnitude of advection to destabilize the constant steady state. This suggests that the population cannot return to previously visited locations too quickly if patterns are to persist. In Case (ii) of Theorem 5.1, we flip the sign of the advection rate and consider the segregation case ($\alpha > 0$), in which case the direction of the monotonicities also switch, but the understanding of this behaviour is identical to Case (i). More interestingly, perhaps, is

the non-monotone behaviour with respect to the memory decay rate μ . In fact, in this case, $\alpha_l(\alpha_r)$ is concave down (up), and so there is a critical value $\mu^* > 0$ so that the rate of advection required to destabilize the constant steady state is minimal. This is in contrast to Theorem 5.2 in Case (ii), where monotonicity with respect to β is lost.

Of particular note is that in classifying the sup/supercriticality of the bifurcation, the sign of $\alpha_n''(0)$ is independent of n in the sense that every bifurcation point leads to a subcritical bifurcation; this is different from Example (ii) below, where the bifurcation will be shown to always be supercritical (see the discussion for Case (ii) below and Figs. 5–6).

Fig. 1 then demonstrates the more complex relationship between the perceptual radius R and the sizes of $\alpha_r(R)$ and $\alpha_l(R)$. Of note is the non-monotone behaviour, particularly for smaller perceptual radii. This wavelike behaviour is most pronounced for $\alpha_r(R)$. It is also easy to see that $|\alpha_l(R)| < \alpha_r(R)$ when $0 < R < \pi/2$ (indeed this holds for $R < 2.2$ from Fig. 1). But when R is larger than 2.2, either $|\alpha_l(R)|$ or $\alpha_r(R)$ could be the larger one. This, in general, shows that the advection rate needed to destabilize the positive equilibrium is larger when the perceptual radius is larger. When the perceptual radius is less than half of the domain size, the attractive advection rate needed to destabilize the positive equilibrium is larger than the repulsive one. In Figs. 2–3, we depict the numerical bifurcation diagrams corresponding to aggregation (Fig. 2) and segregation (Fig. 3), as well as the solution profiles just beyond the critical parameter values.

5.2. Case (ii) in Eq. (1.8.a)

Let $g(u) = \frac{2\rho u^2}{1+u}$ in Eq. (1.8.a). Similar to Case (i), we have

$$\begin{aligned} (u_*, k_*) &= \left(1, \frac{\rho}{\mu + \beta}\right), \quad f_{u*} = -1, \quad f_{u**} = -2, \quad f_{uu*} = 0, \quad g_{u*} = \frac{3\rho}{2}, \\ h_{u*} &= \frac{3\rho\mu + \rho\beta}{2(\mu + \beta)}, \quad h_{k*} = -(\mu + \beta), \quad h_{u**} = g_{u**} = \frac{\rho}{2}, \quad h_{uk*} = -\beta, \\ h_{kk*} &= 0, \quad h_{uu*} = g_{uu*} = -\frac{3\rho}{4}, \quad h_{uuk*} = h_{ukk*} = h_{kkk*} = 0. \end{aligned} \quad (5.8)$$

and

$$\alpha_n(R) = \frac{\text{Det}(J_*) - dh_{k*}n^2}{u_* h_{u*} n^2 \frac{\sin(nR)}{2\pi nR}} = \frac{-2(\mu + \beta)^2}{\rho(3\mu + \beta) \frac{\sin(nR)}{2\pi nR}} \left(d + \frac{1}{n^2}\right). \quad (5.9)$$

After several computations, we find

$$\alpha_n''(0) = \frac{-(632n^4 + 1360n^2 - 72)}{1200C_n(G)n^2}.$$

In contrast to Case (i), we now find that the numerator of the above expression is negative for all $n \geq 1$. Therefore, the sign of $\alpha_n''(0)$ is again determined by the sign of the Fourier coefficients of G , but the conclusions are reversed. At α_l , we check wavenumbers $n \in \Sigma^+$ to find that $\text{sign}(\alpha''(0)) < 0$; by Theorem 4.4 the pitchfork bifurcation is backward and the bifurcating solution is stable. Similarly, at α_r , we check wavenumbers $n \in \Sigma^-$ so that $\text{sign}(\alpha''(0)) > 0$; by Theorem 4.4, the pitchfork bifurcation is forward, and the bifurcating solution is stable. This is precisely what is observed in Figs. 5–6, where a stable small amplitude emerges smoothly from the homogeneous state at precisely the critical values $|\alpha_l|$ and α_r .

The monotonicity of $\alpha_n(R)$ with respect to parameters for Case (ii) is slightly different, so we state the following theorem.

Theorem 5.2. Let $\alpha_n(R)$ be defined in (5.9).

- (i) Suppose $n \in \Sigma^+$ so that $\frac{\sin(nR)}{nR} > 0$. Then $\alpha_n(R) < 0$, and $\alpha_n(R)$ (in particular, α_l) is monotonically increasing with respect to ρ , monotonically decreasing with respect to d , and is not monotone with respect to either μ or β .
- (ii) Suppose $n \in \Sigma^-$ so that $\frac{\sin(nR)}{nR} < 0$. Then $\alpha_n(R) > 0$, and $\alpha_n(R)$ (in particular, α_r) is monotonically increasing with respect to d ,

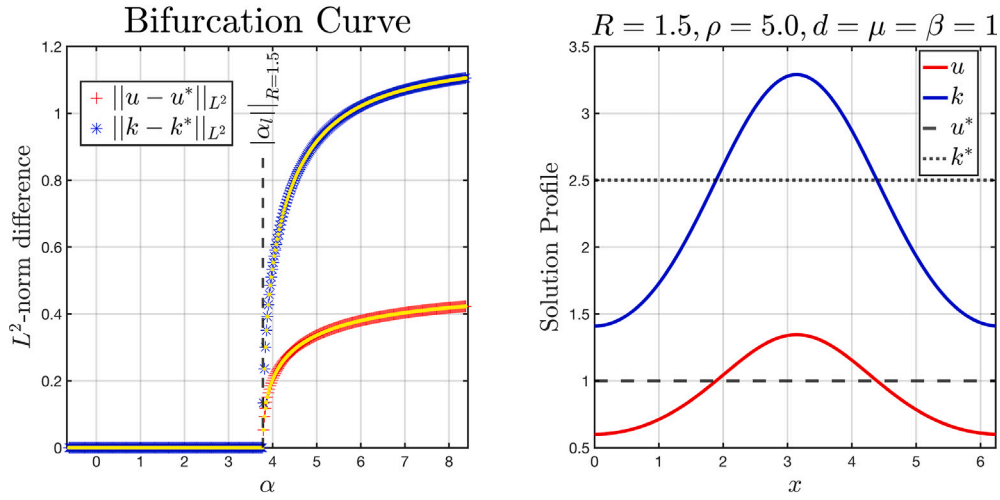


Fig. 5. The bifurcation diagram corresponding to α_r for Example (ii) of Section 5 (left panel) and a sample solution profile ~ 0.1 units beyond the critical threshold $\alpha = \alpha_r(1.5)$ (right panel). Different from Case (i), we now observe a supercritical bifurcation with a low-amplitude solution emerging from the homogeneous state at the critical threshold. The solution profile is similar to Fig. 2, with the notable difference being its amplitude.

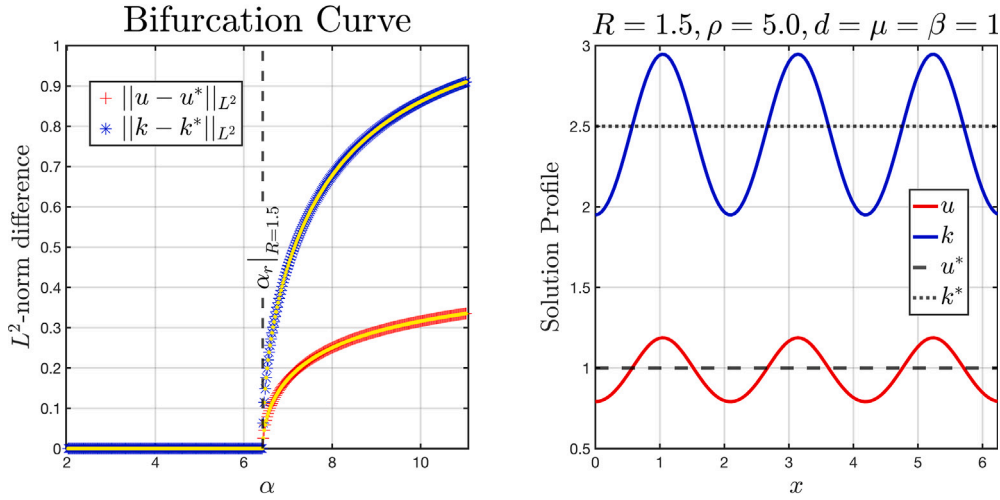


Fig. 6. The bifurcation diagram corresponding to α_r for Example (ii) of Section 5 (left panel) and a sample solution profile ~ 0.1 units beyond the critical threshold $\alpha = \alpha_r(1.5)$ (right panel). The solution profile is similar to Fig. 3, with the same difference noted in Fig. 5: we observe patterns at the same wavenumber as in α_r of Case (i), but now we are able to observe the low-amplitude solution emerging smoothly from the homogeneous state at the critical threshold.

monotonically decreasing with respect to ρ , and is not monotone with respect to either μ or β .

This Theorem, similar to Theorem 5.1 for Case (i), retains the expected monotonicity properties with respect to ρ and d , while we lose monotonicity with respect to β . Indeed, the curves α_l and α_r are concave with respect to each parameter, suggesting the existence of critical values $\mu^* > 0$ and $\beta^* > 0$ so that the magnitude of advection required to destabilize the constant steady state is minimal. This highlights a key difference caused by the choice of memory uptake $g(\cdot)$.

5.3. Case (iii) in Eq. (1.8.b)

In this case, we choose $g(u) = \rho u^2$ in Eq. (1.8.b). From (1.15) and (3.27), bifurcation point $\hat{\alpha}_n(R)$ has the following expression

$$\hat{\alpha}_n(R) = \frac{-(\rho + \mu + \beta)^2}{\kappa \rho (2\mu + \beta) \frac{\sin(nR)}{2\pi n R}} \left(d - \frac{f'(1)}{l_n} \right). \quad (5.10)$$

We again find that bifurcating solutions can only occur in phase with each other.

Similar to Theorem 5.1, we have the following.

Theorem 5.3. Let $\alpha_n(R)$, Σ^+ , Σ^- , α_l , α_r be defined in (1.16) and (5.10). Then there are non-constant steady-state solutions that bifurcation from the constant solution $(1, \frac{\rho\kappa}{\rho+\mu+\beta})$ near $\hat{\alpha}_n(R)$ of system (1.8.b). Moreover, the constant solution $(1, \frac{\rho\kappa}{\rho+\mu+\beta})$ is locally asymptotically stable when $\hat{\alpha}_l < \hat{\alpha} < \hat{\alpha}_r$ and unstable when $\hat{\alpha} < \hat{\alpha}_l$ or $\hat{\alpha} > \hat{\alpha}_r$.

Theorem 5.4. Let $\hat{\alpha}_n(R)$ be defined in (5.10).

- (i) Suppose $n \in \Sigma^+$ so that $\frac{\sin(nR)}{nR} > 0$. Then $\hat{\alpha}_n(R) < 0$, and $\hat{\alpha}_n(R)$ (in particular, $\hat{\alpha}_l$) is monotonically increasing with respect to κ , monotonically decreasing with respect to d , and is not monotone with respect to any of ρ , μ or β ;
- (ii) Suppose $n \in \Sigma^-$ so that $\frac{\sin(nR)}{nR} < 0$. Then $\hat{\alpha}_n(R) > 0$, and $\hat{\alpha}_n(R)$ (in particular, $\hat{\alpha}_r$) is monotonically increasing with respect to d , monotonically decreasing with respect to κ , and is not monotone with respect to any of ρ , μ or β .

We again compare to Theorem's 5.1–5.2: the monotonicity with respect to d remains, while a quadratic growth for the memory uptake function causes all other previously monotone cases to be non-monotone! In Case (iii), we also have a new parameter κ , which is the

theoretical maximal memory capacity of the organism. It is biologically reasonable, therefore, for an increase in this memory capacity to decrease the magnitude of advection required to destabilize the constant steady state.

6. Discussion

The role of spatial memory in driving the movement of animals has long been of interest to both empirical ecologists [1] and mathematical modellers [13]. In this work, we consider the incorporation of a nonlocal advection term in the PDE to model movement in response to remembered space use, where the memory map is described dynamically by an additional ODE. The nonlocal advection term is crucial from both biological and mathematical standpoints [19]. Biologically, it more accurately captures the essence of how organisms sense their surrounding environment and make movement decisions based on that information [17]. This is a useful step forward in our mathematical representation of animal movement ecology, making the modelling formulation more applicable to what is observed in the natural world. Mathematically, however, nonlocality introduces technical difficulties which deserve a careful and robust study.

One of the significant contributions of this paper is the establishment of a well-posedness result, proving the existence and uniqueness of a global solution, ruling out the possibility of a finite-time blowup. In particular, we showed the existence and uniqueness of a solution even when considering the discontinuous top-hat detection function. This result broadens the existing literature in a crucial way, providing answers to some open questions found in [13]. Prior to this work, the existence of solutions for this specific class of models remained an open question. Our result not only bridges this gap but also opens doors for more complex models incorporating different types of detection functions.

Another significant contribution lies in our robust bifurcation and spectral analyses. Previous efforts, motivated more directly by the ecological application, have often relied solely on a linear stability analysis [2,33], which can be insufficient in scenarios where the point spectrum consists of elements with infinite-dimensional kernel. This does not occur in classical reaction–diffusion systems but may occur when nonlocal advection is introduced. Moreover, the comprehensive approach used here reveals a more nuanced understanding of the system's stability, describing more quantitative features of the solution profile near these critical bifurcation points.

From this bifurcation analysis, we establish a number of monotonicity and non-monotonicity results for the critical bifurcation parameters, with the monotonic properties depending on the functional form given chosen for the memory uptake rate $g(\cdot)$. In the special cases considered here, a bounded functional form has the most monotonicity properties, while a roughly linear or quadratic functional form appears to remove most of the monotonicity properties. This suggests the existence of critical values so that the magnitude of advection required to destabilize is minimized, an interesting feature that deserves future study. For example, is the critical value dependent on whether the population aggregates or segregates?

Our numerical simulations using a pseudo-spectral method further complement our analytical results. These numerical methods are particularly well-suited for dealing with nonlocal advection–diffusion problems, demonstrating some of the interesting bifurcation structures of these problems.

While this work provides new insights and fills existing gaps in the literature, further studies are needed to explore more general functional forms, higher-dimensional space, and for domains with a physical boundary. From a biological perspective, there are various aspects of memory at play that are not modelled here [1]. In reality, animals' advective tendencies will not simply be towards (or away from) areas they have previously visited. Rather they will assess the quality of those places – e.g. whether they contain access to food or shelter, if they

have had aggressive or favourable encounters there – and adjust their advective tendencies accordingly [11]. Our work paves the way for analysing these more detailed and realistic memory effects.

One tricky yet important feature will be the inclusion of heterogeneous landscapes, for example, where some areas are better than others for foraging or hiding from predators [4,9]. Analysis of nonlinear PDEs often occurs in a homogeneous environment, but to connect better to the ecological community, theory on pattern formation in heterogeneous environments will be of fundamental importance [53]. Additionally, it will be important to account for between-population interactions via multi-species models with explicit inclusion of memory processes [22]. A possible way into this would be to analyse existing models on territory, some of which are simply multi-species extensions of the model analysed here [7,33], by placing these on solid mathematical foundations through developing existence theory, and gaining greater insights into territorial pattern formation through rigorous spectral and bifurcation analyses.

CRedit authorship contribution statement

Di Liu: Writing – review & editing, Writing – original draft, Investigation, Formal analysis. **Jonathan R. Potts:** Writing – review & editing, Supervision, Methodology, Investigation, Conceptualization. **Yurij Salmaniw:** Writing – review & editing, Writing – original draft, Validation, Investigation, Formal analysis, Conceptualization. **Junping Shi:** Writing – review & editing, Validation, Supervision, Formal analysis. **Hao Wang:** Writing – review & editing, Supervision, Investigation, Conceptualization.

Declaration of competing interest

The authors declare the following financial interests/personal relationships which may be considered as potential competing interests: Di Liu acknowledges research support from the China Postdoctoral Science Foundation (2024M763690). Yurij Salmaniw reports financial support was provided by Natural Sciences and Engineering Research Council of Canada (NSERC Grant PDF-578181-2023). Jonathan R. Potts acknowledges financial support from Engineering and Physical Sciences Research Council (EPSRC) grant EP/V002988/1. Junping Shi reports financial support was provided by National Science Foundation (DMS-1853598 and OCE-2207343). Hao Wang acknowledges research support from the Natural Sciences and Engineering Research Council of Canada (Individual Discovery Grant RGPIN-2020-03911 and Discovery Accelerator Supplement Award RGPAS-2020-00090) and the Canada Research Chairs program (Tier 1 Canada Research Chair Award).

Data availability

No data was used for the research described in the article.

References

- [1] W.F. Fagan, M.A. Lewis, M. Auger-Méthé, T. Avgar, S. Benhamou, G. Breed, L. LaDage, U.E. Schlögel, W.-w. Tang, Y.P. Papastamatiou, et al., Spatial memory and animal movement, *Ecol. Lett.* 16 (10) (2013) 1316–1329.
- [2] B.K. Briscoe, M.A. Lewis, S.E. Parrish, Home range formation in wolves due to scent marking, *Bull. Math. Biol.* 64 (2) (2002) 261–284.
- [3] L. Börger, B.D. Dalziel, J.M. Fryxell, Are there general mechanisms of animal home range behaviour? A review and prospects for future research, *Ecol. Lett.* 11 (6) (2008) 637–650.
- [4] B. Van Moorter, D. Visscher, S. Benhamou, L. Börger, M.S. Boyce, J.-M. Gaillard, Memory keeps you at home: a mechanistic model for home range emergence, *Oikos* 118 (5) (2009) 641–652.
- [5] C. Bracis, T. Mueller, Memory, not just perception, plays an important role in terrestrial mammalian migration, *Proc. R. Soc. B: Biological Sci.* 284 (1855) (2017) 20170449.
- [6] B. Abrahms, E.L. Hazen, E.O. Aikens, M.S. Savoca, J.A. Goldbogen, S.J. Bograd, M.G. Jacox, L.M. Irvine, D.M. Palacios, B.R. Mate, Memory and resource tracking drive blue whale migrations, *Proc. Natl. Acad. Sci.* 116 (12) (2019) 5582–5587.

- [7] J.R. Potts, M.A. Lewis, How memory of direct animal interactions can lead to territorial pattern formation, *J. R. Soc. Interface* 13 (118) (2016) 20160059.
- [8] N. Ellison, B.J. Hatchwell, S.J. Biddiscombe, C.J. Napper, J.R. Potts, Mechanistic home range analysis reveals drivers of space use patterns for a non-territorial passerine, *J. Anim. Ecol.* 89 (12) (2020) 2763–2776.
- [9] J. Merkle, D. Fortin, J.M. Morales, A memory-based foraging tactic reveals an adaptive mechanism for restricted space use, *Ecol. Lett.* 17 (8) (2014) 924–931.
- [10] J.A. Merkle, H. Sawyer, K.L. Monteith, S.P. Dwinell, G.L. Fralick, M.J. Kauffman, Spatial memory shapes migration and its benefits: evidence from a large herbivore, *Ecol. Lett.* 22 (11) (2019) 1797–1805.
- [11] M.A. Lewis, W.F. Fagan, M. Auger-Méthé, J. Frair, J.M. Fryxell, C. Gros, E. Gurarie, S.D. Healy, J.A. Merkle, Learning and animal movement, *Front. Ecol. Evol.* 9 (2021) 681704.
- [12] Q. Shi, J. Shi, H. Wang, Spatial movement with distributed memory, *J. Math. Biol.* 82 (33) (2021) 1–32, <http://dx.doi.org/10.1007/s00285-021-01588-0>.
- [13] H. Wang, Y. Salmaniw, Open problems in PDE models for knowledge-based animal movement via nonlocal perception and cognitive mapping, *J. Math. Biol.* 86 (5) (2023) 1–69, <http://dx.doi.org/10.1007/s00285-023-01905-9>, URL: <https://doi-org.proxy.wm.edu/10.1007/s00285-023-01905-9>.
- [14] Y. Song, H. Wang, J. Wang, Cognitive consumer-resource spatiotemporal dynamics with nonlocal perception, *J. Nonlinear Sci.* 34 (1) (2024) <http://dx.doi.org/10.1007/s00332-023-09996-w>.
- [15] S. Xue, Y. Song, H. Wang, Spatio-temporal dynamics in a reaction-diffusion equation with nonlocal spatial memory, *SIAM J. Appl. Dyn. Syst.* 23 (1) (2024) 641–667, <http://dx.doi.org/10.1137/22M1543860>.
- [16] S. Benhamou, Of scales and stationarity in animal movements, *Ecol. Lett.* 17 (3) (2014) 261–272.
- [17] R. Martinez-Garcia, C.H. Fleming, R. Seppelt, W.F. Fagan, J.M. Calabrese, How range residency and long-range perception change encounter rates, *J. Theoret. Biol.* 498 (2020) 110267.
- [18] N.J. Armstrong, K.J. Painter, J.A. Sherratt, Adding adhesion to a chemical signaling model for somite formation, *Bull. Math. Biol.* 71 (1) (2009) 1–24.
- [19] K.J. Painter, T. Hillen, J.R. Potts, Biological modelling with nonlocal advection diffusion equations, 2023, arXiv preprint [arXiv:2307.14396](https://arxiv.org/abs/2307.14396).
- [20] A.L. Bertozzi, T. Laurent, Finite-time blow-up of solutions of an aggregation equation in R^n , *Comm. Math. Phys.* 274 (2007) 717–735.
- [21] V. Giunta, T. Hillen, M.A. Lewis, J.R. Potts, Detecting minimum energy states and multi-stability in nonlocal advection-diffusion models for interacting species, *J. Math. Biol.* 85 (5) (2022) 1–44, <http://dx.doi.org/10.1007/s00285-022-01824-1>, URL: <https://doi-org.proxy.wm.edu/10.1007/s00285-022-01824-1>.
- [22] J.R. Potts, M.A. Lewis, Spatial memory and taxis-driven pattern formation in model ecosystems, *Bull. Math. Biol.* 81 (2019) 2725–2747.
- [23] L. Harten, A. Katz, A. Goldshtein, M. Handel, Y. Yovel, The ontogeny of a mammalian cognitive map in the real world, *Science* 369 (2020) 194–197.
- [24] M. Peer, I. Brunec, N. Newcombe, R. Epstein, Structuring knowledge with cognitive maps and cognitive graphs, *Trends Cogn. Sci.* 25 (1) (2021) 37–54.
- [25] J.R. Potts, L. Börger, B.K. Strickland, G.M. Street, Assessing the predictive power of step selection functions: How social and environmental interactions affect animal space use, *Methods Ecol. Evol.* 13 (8) (2022) 1805–1818.
- [26] M. Lewis, J. Murray, Modelling territoriality and wolf-deer interactions, *Nature* 366 (6457) (1993) 738–740.
- [27] P.R. Moorcroft, M.A. Lewis, R.L. Crabtree, Mechanistic home range models capture spatial patterns and dynamics of coyote territories in Yellowstone, *Proc. R. Soc. B: Biological Sci.* 273 (1594) (2006) 1651–1659.
- [28] C.S. Holling, The functional response of predators to prey density and its role in mimicry and population regulation, *Memoirs Entomol. Soc. Can.* 97 (S45) (1965) 5–60.
- [29] W.F. Fagan, E. Gurarie, S. Bewick, A. Howard, R.S. Cantrell, C. Cosner, Perceptual ranges, information gathering, and foraging success in dynamic landscapes, *Amer. Nat.* 189 (5) (2017) 474–489.
- [30] S. Lima, P. Zollner, Towards a behavioral ecology of ecological landscapes, *Trends Ecol. Evol.* (1996).
- [31] C. Krebs, Ecological methodology, in: *The Benjamin/Cummings Series in the Life Sciences*, Benjamin/Cummings, 1999, URL: <https://books.google.pt/books?id=1GwVAQAIAAJ>.
- [32] A. Boonman, Y. Bar-On, Y. Yovel, It's not black or white—on the range of vision and echolocation in echolocating bats, *Front. Physiol.* 4 (2013).
- [33] J.R. Potts, M.A. Lewis, Territorial pattern formation in the absence of an attractive potential, *J. Math. Biol.* 72 (1–2) (2016) 25–46, <http://dx.doi.org/10.1007/s00285-015-0881-4>, URL: <https://doi-org.proxy.wm.edu/10.1007/s00285-015-0881-4>.
- [34] K. Painter, V. Giunta, J. Potts, S. Bernardi, Variations in non-local interaction range lead to emergent chase-and-run in heterogeneous populations, *J. R. Soc. Interface* (2024).
- [35] A. Ducrot, X. Fu, P. Magal, Turing and turing-Hopf bifurcations for a reaction diffusion equation with nonlocal advection, *J. Nonlinear Sci.* 28 (5) (2018) 1959–1997, <http://dx.doi.org/10.1007/s00332-018-9472-z>.
- [36] V. Giunta, M.C. Lombardo, M. Sammartino, Pattern formation and transition to chaos in a chemotaxis model of acute inflammation, *SIAM J. Appl. Dyn. Syst.* 20 (4) (2021) 1844–1881, <http://dx.doi.org/10.1137/20M1358104>, URL: <https://doi-org.proxy.wm.edu/10.1137/20M1358104>.
- [37] A. Jüngel, S. Portisch, A. Zurek, Nonlocal cross-diffusion systems for multi-species populations and networks, *Nonlinear Anal.* 219 (2022) 112800–112826, <http://dx.doi.org/10.1016/j.na.2022.112800>, URL: <https://doi-org.proxy.wm.edu/10.1016/j.na.2022.112800>.
- [38] J. Shi, C. Wang, H. Wang, X. Yan, Diffusive spatial movement with memory, *J. Dynam. Differential Equations* 32 (2) (2020) 979–1002, <http://dx.doi.org/10.1007/s10884-019-09757-y>.
- [39] Y. Song, J. Shi, H. Wang, Spatiotemporal dynamics of a diffusive consumer-resource model with explicit spatial memory, *Stud. Appl. Math.* 148 (1) (2022) 373–395, <http://dx.doi.org/10.1111/sapm.12443>, URL: <https://doi-org.proxy.wm.edu/10.1111/sapm.12443>.
- [40] A. Marciniak-Czochra, G. Karch, K. Suzuki, Instability of turing patterns in reaction-diffusion-ODE systems, *J. Math. Biol.* 74 (3) (2017) 583–618, <http://dx.doi.org/10.1007/s00285-016-1035-z>.
- [41] Y. Li, A. Marciniak-Czochra, I. Takagi, B. Wu, Bifurcation analysis of a diffusion-ODE model with turing instability and hysteresis, *Hiroshima Math. J.* 47 (2) (2017) 217–247, URL: <http://projecteuclid.org/euclid.hmj/1499392826>.
- [42] J.A. Carrillo, Y. Salmaniw, J. Skrzeczkowski, Well-posedness of aggregation-diffusion systems with irregular kernels, 2024, [arXiv:2406.09227](https://arxiv.org/abs/2406.09227).
- [43] J.A. Carrillo, R.S. Gvalani, G.A. Pavliotis, A. Schlichting, Long-time behaviour and phase transitions for the mckean-vlasov equation on the torus, *Arch. Ration. Mech. Anal.* 235 (1) (2020) 635–690.
- [44] J.A. Carrillo, K. Craig, Y. Yao, Aggregation-diffusion equations: dynamics, asymptotics, and singular limits, in: *Active Particles. Vol. 2. Advances in Theory, Models, and Applications*, in: *Model. Simul. Sci. Eng. Technol.*, Birkhäuser/Springer, Cham, 2019, pp. 65–108.
- [45] O. Ladyzhenskaiâ, V.O.A. Ladyženskaja, V. Solonnikov, N. Uraltseva, U. N.N., Linear and quasi-linear equations of parabolic type, American Mathematical Society, translations of mathematical monographs, American Mathematical Society, 1968, URL: <https://books.google.ca/books?id=HsE-AAAAIAAJ>.
- [46] V. Bogachev, N. Krylov, M. Röckner, S. Shaposhnikov, Fokker-Planck-Kolmogorov equations, *Mathematical Surveys and Monographs*, American Mathematical Society, 2015, URL: <https://books.google.pt/books?id=z9FYCwAAQBAJ>.
- [47] L.H. Wang, A geometric approach to the Calderón-Zygmund estimates, *Acta Math. Sin. (Engl. Ser.)* 19 (2) (2003) 381–396, <http://dx.doi.org/10.1007/s10114-003-0264-4>, URL: <https://doi-org.proxy.wm.edu/10.1007/s10114-003-0264-4>.
- [48] Z. Wu, J. Yin, C. Wang, Elliptic & parabolic equations, World Scientific Publishing Co. Pte. Ltd., Hackensack, NJ, 2006, p. xvi+408, <http://dx.doi.org/10.1142/6238>, URL: <https://doi-org.proxy.wm.edu/10.1142/6238>.
- [49] P. Magal, S. Ruan, Theory and applications of abstract semilinear Cauchy problems, *Applied Mathematical Sciences*, vol. 201, Springer, 2018, http://dx.doi.org/10.1007/978-3-030-01506-0_xvii+543. With a foreword by Glenn Webb.
- [50] M.G. Crandall, P.H. Rabinowitz, Bifurcation from simple eigenvalues, *J. Funct. Anal.* 8 (1971) 321–340, [http://dx.doi.org/10.1016/0022-1236\(71\)90015-2](http://dx.doi.org/10.1016/0022-1236(71)90015-2).
- [51] M.G. Crandall, P.H. Rabinowitz, Bifurcation, perturbation of simple eigenvalues and linearized stability, *Arch. Ration. Mech. Anal.* 52 (1973) 161–180, <http://dx.doi.org/10.1007/BF00282325>.
- [52] J.P. Shi, Persistence and bifurcation of degenerate solutions, *J. Funct. Anal.* 169 (2) (1999) 494–531, <http://dx.doi.org/10.1006/jfan.1999.3483>.
- [53] A.L. Krause, V. Klika, T.E. Woolley, E.A. Gaffney, From one pattern into another: analysis of turing patterns in heterogeneous domains via WKBJ, *J. R. Soc. Interface* 17 (162) (2020) 20190621.